Pitfalls in Ion Beam Analysis

C.Jeynes and N.P.Barradas

University of Surrey Ion Beam Centre, Guildford GU2 4JE, England

Instituto Tecnológico e Nuclear, 2686-953 Sacavém, Portugal

This work is a revision of, and incorporates part of the previous 1992 IBA Handbook (the "Black Bible") chapter 12 by J. A. Davies, W. N. Lennard and I. V. Mitchell. The section on electronic noise is by Max Döbeli (Zurich)

17th June 2009

Table of Contents

Glossary

IBA: Ion beam analysis
RBS: Rutherford backscattering spectrometry
EBS: Elastic (non-Rutherford) bascscattering spectrometry
ERD: Elastic recoil detection (also ERDA = ERD analysis; FRS = forward recoil spectrometry)
NRA: Nuclear reaction analysis
PIXE: Particle induced X-ray emission
PIGE: Particle induced γ-ray emission

1 Introduction

IBA is a quantitative analytical technique, and in this chapter we intend to show how to avoid many pitfalls when determining elemental depth profiles accurately with light ion RBS using MeV ion beams. IBA can of course use various other beams, and for a variety of other purposes, including profiling of crystalline defects. This present discussion is usually, but not always, easily generalised to these other cases: we will therefore also cover pitfalls in a number of other important examples.

We will in general be guided by the previous IBA Handbook Chapter 12 (by Davies, Lennard & Mitchell). However, this has many subtle discussions that we will avoid or simplify, referring the advanced IBA user back to it. Today most laboratories that are starting to use IBA have the new generation of accelerators, eliminating many of the problems associated with the older accelerators which the previous chapter addressed.

There is a new generation of software available which renders obsolete many of the numerical examples of the previous Handbook. We will assume that users interested in accurate work will have access to one of the codes described and evaluated in the recent International Atomic Energy Agency (IAEA) sponsored IBA software intercomparison exercise (Barradas *et al*., 2007) where it is shown that IBA spectra can be treated numerically with a confidence of about 0.2%, and that currently the best absolute experimental accuracy available is 0.6%. We therefore intend to describe sources of error (pitfalls) greater than about ¼%: we think users should be aiming at accuracies of 1% or better.

The nuclear physics background of the old generation of IBA practitioners has become inaccessible to many of today's users; IBA is of great value in materials characterisation and is used increasingly by materials scientists who have not had a nuclear physics training. This chapter is intended to be of particular value to this type of user.

Accurate elemental depth profiling by IBA is of great value in many modern thin film technologies: the most obvious comparable technique is SIMS (secondary ion mass spectrometry) which is often used for these types of problems. SIMS is a powerful and sensitive technique, but it is usually only semi-quantitative, and it is generally unreliable at interfaces (unless the system is well known). IBA, on the other hand, is particularly good at interfaces, and has an accuracy that is easily traceable to international standards, making it suitable for standards work. We will show in this chapter how to best capitalise on these strengths.

For parts of this chapter we will take a measurement of the implanted fluence of As into Si (Jeynes *et al.,* 2006) as a worked example of various pitfalls in doing accurate IBA. The collected spectra are shown in Fig.1. There are two important equations relevant to this discussion: Eq.1 simply describes the number N_A (in atoms/cm^2) of As atoms, which is given by the measured area A_A of the signal of element A (in this particular example A is As) (in counts):

$$A_A = Q\, N_A\, \sigma'_A\, (E, \theta)\ \ \Omega \qquad (1)$$

where Q is the number of incident particles (the "collected charge") and Ω is the detector solid angle (in steradians sr). σ'_A is the differential cross-section (in cm^2/sr) of element A and is a function both of the scattering angle θ and of the beam energy E as it decreases from its initial energy E_0 as it penetrates into the sample.

In Fig.1 there are two signals of analytical interest. The first is obviously the As signal. However, in Eq.1 we also need to know the charge.solid-angle product $Q\Omega$. This is determined from the Si signal and the known energy loss of the He beam in a silicon matrix. For backscattering with the detector at an angle of θ to the beam and normal beam incidence the surface yield Y_0 (in counts/channel) for element A in a matrix AB is given by Eq.2:

$$Y_{0,A} = Q\, f_A\, \sigma'_A\, \Omega\, \Delta / [\, \varepsilon_0 \,]_A^{AB} \qquad (2)$$

where f_A is the fraction of the matrix that is element A, Δ is the electronic gain (in eV/channel of the analogue-digital converter), and $[\, \varepsilon_0 \,]_A^{AB}$ (in $eV.cm^2$) is the energy loss factor for the signal of A from the surface of matrix AB given the beam energy and the scattering angle (see Ch.**3**).

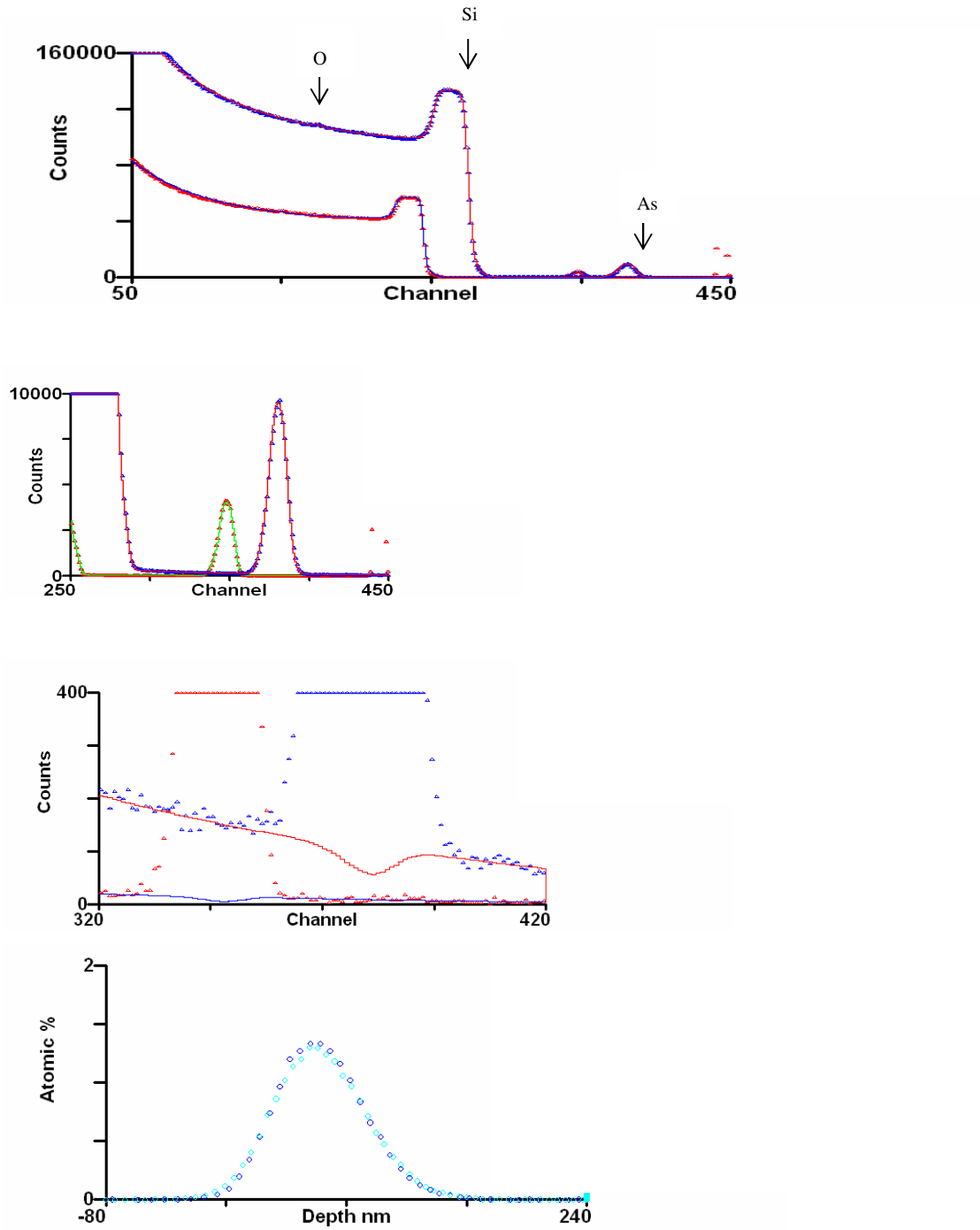

Figure 1: Accurate analysis of As implanted fluence in Si. *(Above) Nominal implant 5.10^{15} As/cm^2 at 100keV. 1.5MeV He RBS spectra from two detectors collected simultaneously and 0.5mC collected charge, with fits. The beam is incident normally on the sample such that it channels in the substrate, and the near-surface region of silicon amorphised by the ion beam is clearly seen. A small O peak from the surface oxide is also clearly distinguishable. The As, Si and O edges are marked for the larger solid angle detector (Upper Middle) Detail of the As signal. (Lower Middle) Expanded detail of the As signal, with the non-linear pileup correction function shown. (Below) Pileup corrected As signal from each detector plotted on concentration vs depth scale (using Si density of 5.10^{22}/cc) (Reproduced from Jeynes et al 2006)*

Eqs.1&2 have been simplified without any loss of generality. They should both really be integrals over the depth of the signal, noticing that σ' varies as $1/E^2$, and that $[\varepsilon]$ is also a function of depth. The standard IBA codes have been validated to do these integrations correctly (Barradas *et al*., 2007).

For the example of Fig.1, determining the number of As atoms present (using Eq.1) depends on an indirect measurement of the charge.solid-angle product $Q\Omega$ from the height Y of the silicon substrate signal (using Eq.2), where the number of Si scattering centres is implicit in the $\Delta/[\varepsilon]$ ratio. In the rest of this chapter we will elaborate on various of the issues raised (as well as some others).

2 Lost Beam and Events

2.1 Charge Measurement

The collected charge Q in Eqs.1&2 is a very important quantity which it is not so easy to measure. In the implantation of Fig.1 the As implanted fluence was determined during the implantation by collecting charge in Faraday cups of a design shown in Fig.2. This is a demanding application since large heavy-ion beam currents are used in implanters and the beam being measured usually falls only partially on the primary aperture. Jeynes *et al*. (2006) shows that this design is capable of charge measurement in this application with an accuracy around 1%.

At issue is not the simple measurement of charge in a current integrator which can (and should!) be calibrated against standard current sources with pC accuracy. There are two points to note from Fig.2. Firstly, the incident beam will generate a large number of secondary electrons at the primary (beam defining) aperture (P), many of which will have a significant momentum towards the target. The secondary electron current is usually comparable to the incident beam current; and often exceeds it, in the case of a heavy ion beam, by orders of magnitude. It is important to carefully suppress such electrons.

Secondly, the beam striking the target will liberate many secondary electrons and photons (X-rays). Most of the secondary electrons will be low energy (<10eV), but there are a significant number of high energy electrons, which may have keV energies. Some electrons will therefore escape the Faraday cup (S) through the secondary aperture (A, this aperture is not struck by the primary beam) and must be suppressed. There is also a possibility that secondary positive ions (or low energy multiply scattered primary ions) may also escape the Faraday cup: these will be attracted by the suppression electrode and will give rise to tertiary currents (which will be amplified by secondary electrons liberated and repelled from the suppression electrode by the ion impacts). Tertiary currents are not seen by the current integrator (I) in this design. These secondary particle effects may be very large for some insulating samples and at low (keV) beam energies.

For IBA applications such a well designed Faraday cup is usually impractical, since the target may be large or part of a more or less complicated manipulator; and in any case access is needed for detectors which may be of various types (particle, photons including X-rays, ToF etc) or in various geometries. But when direct charge measurements are made the geometry of the actual apparatus should be critically compared with the "ideal" Faraday cup described. It should be remembered that photon impact can also liberate secondary electrons, and for samples which generate many photons this effect may be large (Venkatesan, 1984).

Electron suppression can work just as well with magnetic as with electrostatic fields, and small, strong permanent magnets are now readily available. But the use of electrostatic and magnetic fields together is to be avoided since when both fields are present electron paths can be very complicated and any possible escape paths will probably be found. With electrostatic fields the suppressor action should be checked periodically since insulating deposits can build up on the surfaces over time, attracting fixed charges that can entirely compensate the applied field.

A variety of methods have been used to determine collected charge apart from direct measurement from the target. A transmission Faraday cup has been described by Sitter *et al.* (1982), and by Pászti *et al.* (1990). In both of these instruments a rotating or reciprocating vane cuts the beam periodically and the charge deposited on the vane is measured with a precision of about 1%. The pitfall to avoid in this sort of measurement is to forget that the secondary electron yield is enormous when the beam strikes the edge of the vane, and that suppression of these electrons is as important on the downside as on the upside of the vane. A passive instrument where a fixed mesh is used instead of a chopper has been described by El Bouanani *et al* (2006).

A rotating vane instrument has been reported by Piel *et al* (1994), and by Giuntini & Mando (1994) where backscattered particles instead of charge are collected from the vane. For these instruments the vane is coated with gold and the particles scattered from gold are discriminated in a SCA (single channel analyser). This is quite a troublesome arrangement since the signal changes for different beams and you really need to see the spectrum to set up the SCA correctly. Users have also found that they need to use a gate to exclude edge signals from the detector. It is possible, but not easy, to obtain excellent precision (1%).

Transmission detectors take a fraction of the beam of course, and this fraction must be measured directly with a downstream Faraday cup (which can be of ideal design). The great virtue of transmission detectors is that they are completely independent of the target, which can then be manipulated, be heated or cooled, or be of any material without any effect on the charge measurement.

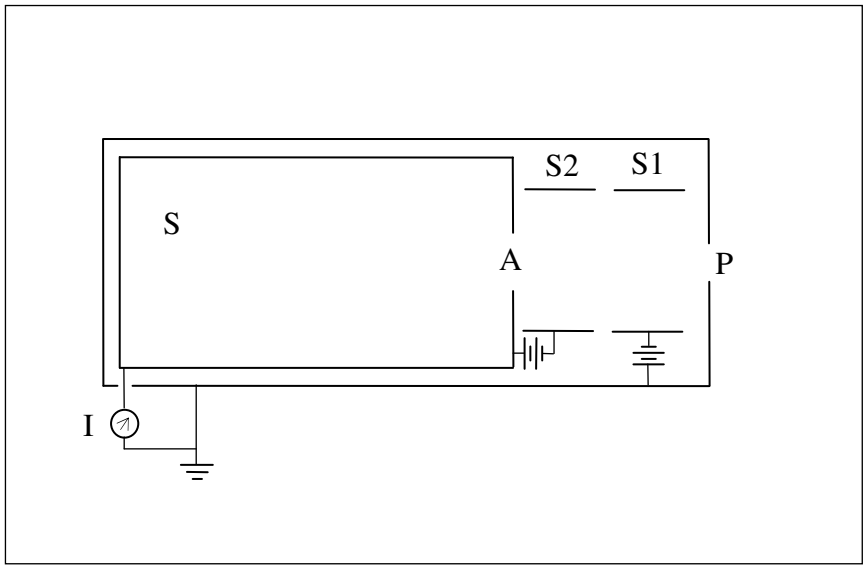

Figure 2: Faraday Cup Design. *The sensor S is an equipotential volume in an earthed case. Secondary electrons from the primary aperture P are suppressed by the electrode S1, and any secondary electrons escaping through the secondary aperture A are suppressed by the electrode S2. Suppression voltages are typically 300V.*

2.2 Beamline Charge Exchange

In modern systems with good vacuum this is an unusual problem. Users should however be aware that there is a possibility of significant beam charge exchange where the vacuum is poor. This has been reviewed in considerable detail by Allison (1958). There is a probability both of lower and higher charge states.

Accelerators used for implantations often scan the ion beam to implant the sample uniformly, and in these beam lines a "neutral trap" is always incorporated: this is a voltage applied to transmit the beam past a kink in the beam line. The neutral beam is not deflected and is intercepted by an

aperture. For IBA the beam lines do not always have neutral traps and the beams are not usually scanned so that neutral beams will give an unchanged IBA signal but will not be detected by the current integrator. Since the beam lines are usually long the neutral fraction of the beam may be significant if the vacuum is poor.

Conversely, a He^+ beam may suffer further charge stripping collisions, giving a significant He^{++} component. As an example, if the beam line pressure is 1mPa (10^{-5}mbar) and the beamline is 4m long the neutralisation probability for a 450keV $^4He^+$ particle will be about 1%, but the probability of stripping to He^{++} is *higher* at about 2%. For a 450keV He^{++} beam in this beam line the probability of He^+ is 5% but the probability of the neutral is only 0.5%. For three times the energy one might expect the neutralisation cross-sections to fall by a factor 3 or so. The cross-section for He^+ to change to He^{++} falls from 66Mbarns to 37Mbarns as the He^+ energy increases from 450keV to 1700keV, but the reverse charge exchange, of He^{++} changing to He^+, falls from 170Mbarns (for 450keV He^{++}) to 5Mbarns (for 1700keV He^{++}).

2.3 Particle Identification

A precise knowledge of the incident particle parameters is essential for all ion beam experiments. We assume here that the accelerator has only an analyzing magnet (with relatively poor mass resolution compared to AMS - accelerator mass spectrometry) to perform momentum selection of the beam. Many accelerators suffer from periodic problems due to unwanted contaminant beams that arrive at the target together with the desired species. Such problems are caused by:

- Atomic or molecular particles whose kinematic properties mimic the acceleration and deflection kinematics of the desired particle;
- Unwanted particles that reach the target because of a low probability charge exchange sequence occurring upstream of the target; or
- Particles that have completely incorrect kinematics but arrive at the target because of (wall) scattering.

One of the simplest ways to test for a mixture of 'equal-mass' beams in single-ended machines is to detect elastically scattered projectiles from a thin self-supporting Au target. An energy spectrum analysis with a standard surface barrier detector system will readily distinguish the fragments of molecular impurities, such as mixtures of H_3^+, HD^+ and $^3He^+$, or $^4He^+$ and D_2^+, which may arise through ion source memory effects.

The consequence of scattering the three ion species, H_3^+, HD^+, and $^3He^+$, from a thin Au scattering foil, when the incident species have equal energy (1 MeV), is shown in Table 1. We assume that the detector is located at 90° (lab. angle). The three beams would give rise to three distinct peaks:

- For H_3^+, a single peak at 0.33 MeV energy;
- For HD^+, two peaks corresponding to 0.33 MeV protons and 0.67 MeV deuterons; and
- For $^3He^+$, a single peak at 1 MeV energy.

The relative intensities are distinctive. The entries in Table 1 are based on a simple $(Z_iZ_j/E)^2$ dependence of the elastic (Rutherford) cross section for the dissociated fragments, and approximating the kinematical factors by unity.

Another example of the use of this Au foil scattering technique is the identification of ^{16}O ions in the presence of ^4He ions — a curiosity observed by Hemment *et al.,* (1975) when poor beamline vacuum developed, thereby allowing a $^{16}O^+$ impurity beam co-accelerated to 2 MeV with the $^4He^+$ beam to charge-exchange to $^{16}O^{++}$ in the drift section between the accelerator and the analyzing magnet. This process allowed two beams of 'identical' rigidity, $ME/q^2 = 8$ (MeV-amu), to be passed by the magnet.

Table 1: Relative particle yields and energies for several "mass 3" ions incident on "Au" at 1MeV			
	Relative yield for scattered particle(s)		
Beam	**H 0.33MeV**	**D 0.67MeV**	**^{3}He 1.0MeV**
H_3^+	27		
HD^+	9	2.25	
$^3He^+$			4

The molecular interferences are not problematic for tandem-type accelerators, where there is an injection magnet at the source, an analyzing magnet following acceleration, and a (collisional) stripping event at the high voltage terminal.

Wall scattering can be minimized using a series of apertures; however, care must be exercised so as not to restrict beamline pumping speed excessively.

2.4 Deadtime and Pulse Pileup

We restrict our comments to 'singles' experiments (as opposed to coincidence experiments) and solid state detectors, which are most common for ion beam analysis applications, although much of this section is common to all types of analysis.

Deadtime is generated in the counting system by the time taken to process each pulse. This is typically dominated by the ADC conversion time (of the order of 10μs) for particle detectors and by the preamplifier pulse processing time for Si(Li) X-ray detectors (typically greater than 10μs). In all systems the ADC should be capable of reporting the actual dead time for each counting channel to the user. This dead time must include any time spent in handshaking between the various electronic components. Where the ADC is multichannel or where the host computer is multitasking there may be significant extra system deadtime that affects all channels. In any case, where multiple detectors are used simultaneously it is more important to accurately determine the relative live charge between the detectors than it is to determine the charge that fell on the sample (the true charge) during the collection time. For accurate work it is essential to understand the operation of your spectroscopy system in detail.

Pulse pileup occurs when separate pulses come too close together in time and are not recognised as separate by the spectroscopy system. There are two cases: whether or not a pileup rejection (PUR) circuit is present. Where PUR is used pileup events will still occur since every spectroscopy system has a pulse detection time resolution, and there is a non-zero probability for pulses to occur at any time separation, even simultaneously. Surface barrier detector preamplifiers for example can have a rise time of about 30ns, and a typical resolution time for an amplifier PUR circuit is 500ns. However, where PUR is used any pileup events that are not rejected are "nearly" simultaneous, that is, the amplitude of the resulting sum pulse is nearly the sum of the amplitudes of the pileup pulses. Where PUR is not used the sum pulse may be of (nearly) any amplitude.

It is possible to almost entirely eliminate pileup by determining the momentum of the detected particles as well as their energy using a ΔE-E detector telescope (Gurbich, 1996) or using a time of flight detector with a pulsed incident ion beam (Gurbich & Kornilov, 1991). However, these have significantly greater complexity, and the ΔE/E method needs very thin ΔE detectors for lower

energy He beams. We will concentrate here on correcting spectra collected with the simplest detectors.

Fig.3 shows a spectrum with significant pileup (and with PUR). The Au signal appears at ch150 and the electronic pulser signal at ch480. All the counts above the Au signal are pileup counts (except for the pulser), and the shape of the pileup signal is recognisably an autoconvolution of the spectrum. The 2-pulse pileup is accurately calculated (with or without PUR) with the algorithm of Wielopolsky & Gardner ("W&G", 1979). This is a slow calculation, involving $n_{channel}^3$ operations: the autoconvolution method (van Lieshout, 1966), improved by Amsel *at al* (1992), is faster given that it involves only $n_{channel}^2$ operations, but not so accurate. Where the pileup correction is significant, the best calculation should be done: refer to the Manual for the IBA code being used. Some codes will also make an approximate calculation of 3-pulse pileup (e.g. Barradas & Jeynes, 2008). We note that the best pileup calculations for most current PIXE codes do not use the best algorithms (Barradas & Reis, 2006). We note also that the W&G algorithm assumes parabolic-shaped pulses, but can be extended to other shapes as well, and requires knowledge of the time for a pulse to reach the maximum, which depends on the amplifier used (normally given in the amplifier documentation).

The W&G algorithm is used in Fig.1c to determine the pileup correction function of the As signal. This figure illustrates a dangerous pitfall: you might think that this pileup background is nicely linear from the pileup behaviour above and below the signal. But it is very clear from the calculated pileup signal shown that the pileup is actually strongly non-linear. Of course, the pileup at any channel is the sum of the pileup events that are detected in that channel and events which should be in that channel but which are actually piled up and end up in higher channels. For strong signals the pileup background can be *negative* since the latter events outweigh the former. For example, the Au signal of Fig.3 is *underestimated* by 1.5% even for the relatively low count rate of 4kHz.

Notice in Fig.3 that below about ch30 there is a large "noise" signal. Usually this is discriminated by the LLD (lower level discriminator) of the amplifier to reduce the count rate into the ADC, but pileup will occur anyway whether or not the (real) counts appear in the spectrum. In this case the LLD was on, but an assumed (*ad hoc*) signal was arbitrarily included in the spectrum shown such that the pileup above the Au edge and above the pulser signal were correctly reproduced. The extra (unfitted) counts above about ch505 are an artefact of the ADC which integrates all the high energy counts instead of truncating them. The pitfall to avoid is relying on even a good pileup calculation such as W&G too near a leading edge where the LLD will distort the calculated pileup signal.

When doing accurate work that depends on a good pileup calculation it is important to use a constant beam current. The algorithms used by the IBA codes take the live time as the input from which average count rate is calculated. If the count rate fluctuates the pileup cannot be accurately calculated. The W&G calculation has no free parameters, although the collection time, the shaping time and the PUR time resolution can be treated as fitting parameters. Analysts should note that the large, rapid fluctuations in the incident beam intensity described by Sjöland *et al* (1999) invalidates the simple W&G calculation and every effort should be made to avoid fluctuating beams. Thankfully, modern accelerators generate a very constant beam current. Sjöland *et al.* also describe the more difficult case of scanning microbeam PIXE, where even if the beam current is constant, the count rate is not in general.

Deadtime and pileup arise in all of the electronic components: preamplifier, amplifier, ADC, etc., due to the pulse rate. Solid state detectors should be operated at pulse rates where the pulses are separated by an average time interval that is much more than the deadtime inherent in the rest of the electronic circuitry. A 10μs dead time per pulse implies a maximum counting rate of 100kHz, but of course the pulses come randomly in time and dead time will increase rapidly (and non-linearly) for count rates higher than about 10kHz.

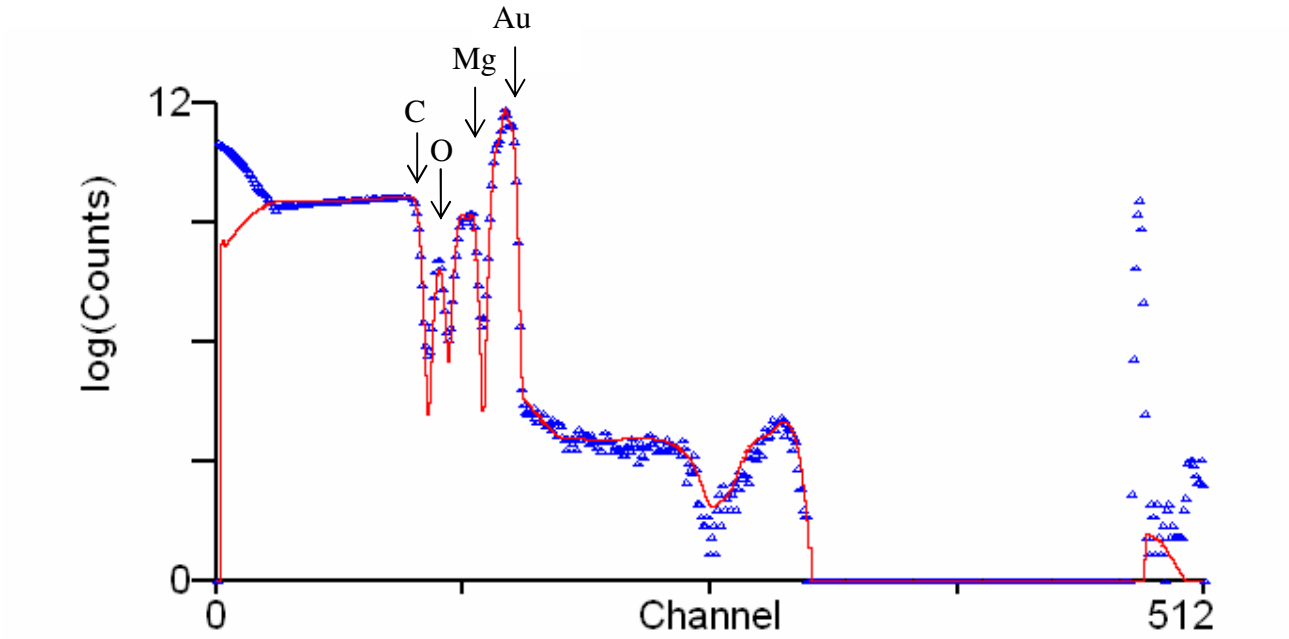

Figure 3: Pileup with pileup rejection. *707keV $^1H^+$ RBS of a Au/Mg multilayer on C, 4.3kHz count rate, amplifier shaping time 500ns, PUR time resolution 550ns. A distinct O contamination peak can also be seen. Fit including pileup calculated with Wielopolsky & Gardner's algorithm is in red.*

It is a good practice to *always* use a test pulse (see the pulser signal at ch480 of Fig.3) at the appropriate preamplifier input, that is, introducing a signal which is periodic with known frequency (typically about 60 Hz). Thus, the total number of 'missing' pulses due to count rate losses during an acquisition time can be calculated from the *measured* area under the pulser peak. If the pulser is gated for dead time then it will reflect pileup losses. When using a Faraday cup that rotates into the beam periodically there are no pulser losses when the beam is hitting the cup. Here the precise duty cycle of the cup must be measured and its effect factored into the correction. Another way to measure counting losses using a pulser is to trigger the pulser with an output (usually scaled) from the current integrator. This way, if the beam goes off, so do the pulses, and since one usually counts for a preset charge, the number of pulses is also known. The pulser is in any case valuable to monitor the electronics stability during the data collection run, and to monitor the noise performance of the system.

In general, counting rate losses will be non-negligible for total pulse counting rates exceeding 1kHz, which applies to almost all RBS measurements. Raising the LLD of the amplifier and/or ADC can decrease the deadtime problem, provided that the low energy region of the spectrum is extraneous to the experiment (but this will also distort the pileup calculation as described above). See Knoll's excellent text (1989) for more detail.

To conclude this section we urge the reader to avoid the pitfall of counting *too slowly* in an attempt to avoid pileup and dead time effects. It is a misuse of spectroscopic electronics of excellent linearity and of highly expensive accelerator facilities not to count as fast as is feasible. We emphasise that the W&G pileup calculation is *exact* for 2-pulse pileup (for parabolic pulses), and good quality electronics will also give very precise dead time values, so there is no need to reduce the count rate to avoid these effects except, of course, where the signal/noise ratio is critical such as when looking for trace heavy elements in a light matrix where the background is all from pileup. In any case there are diminishing returns for decreasing the counting rate since pileup is linear with counting rate and so is deadtime for low count rates.

Count fast and do the corrections correctly!

2.5 Electronic Noise and Ground Loops

State-of-the-art ion implanted silicon detectors reach an energy resolution of 10 keV (FWHM: full-width-half-maximum) for helium ions and 5 keV for protons. The contribution of electronic noise from a standard preamplifier is about 3 keV. For high resolution measurements it is therefore important to avoid the pick-up of any other disturbance from the electromagnetic environment. If gas ionization chambers are used the charge produced per keV particle energy can be more than a factor of 6 lower than in a silicon detector and electronic noise becomes more important by this same factor. If capacitive noise from the preamplifier is the limiting contribution to the resolution the performance can be improved by reducing the capacitance of the detector and connecting cable and by using a preamplifier with cooled FET (field effect transistor). If the specified noise level (measured by a precision pulser) is not obtained there is most certainly periodic noise involved. Additional information can be found in Goulding & Landis (1982), Radeka (1988), and Morrison (2007).

To track and remove periodic noise can be very tedious and there is no single recipe that reliably leads to success. Basically there are two strategies: on the one hand to remove the sources of noise and on the other hand to improve shielding and reduce sensitivity of the detector chain against the disturbance. In the following we list tests that can be done and measures that can be taken. It has to be mentioned that some actions that improve conditions in one situation may be detrimental in another one, depending on the electrical grounding scheme used and the nature of the noise source.

- Check cable shieldings and connectors, especially the ground lead of the preamplifier input connector has to be firm (check by careful twisting). Do not use unnecessarily long cables.
- Beamlines and vacuum vessels are not necessarily good conductors and on a well defined ground potential. Try to connect the flange which carries the electrical feedthrough to the detector with a solid copper cable to the electrical ground of detector electronics.
- Extra ground cables have to be of large cross-section (rather 10 than 1 mm^2) and connected firmly. If other cables carry ground along the same line, avoid producing ground loops and slightly twist cables around each other.
- If you have three-phase electrical power in the laboratory that is split up into three two-phase current networks never mix phases for one experimental set-up. Acquisition electronics (including data-taking computers) should be powered by the same phase. If necessary install an extra power cable to computer or control room.
- If possible try "star grounding" of your electronics to avoid ground loops, i.e. there is only one single connection to ground potential in the whole system. In this case the shielding of the detector cable has to be insulated from the vacuum vessel.
- Avoid strong high frequency emitters close to the experiment. These are often chopped power supplies, turbopump controllers, PC-monitors, etc. If emitters are inside the vacuum vessel (as e.g. turbopumps) the detector may act as an antenna: rethink the shielding scheme.
- To track the sources of periodic noise run a fast Fourier-Transform on an oscilloscope. In some cases a simple ferrite filter can help.
- Microphonic noise (i.e. mechanical vibrations of the detector) can produce similar disturbances. If produced by a turbopump it can even have the same frequency as the noise induced by the electromagnetic field.

3 Fixed Parameter Calibration

In Eq.1 the unknown experimental parameter is the product of the charge Q and the solid angle Ω. The measurement of charge has been treated above. In Eq.2 the electronics gain Δ appears as well as the charge.solid-angle product $Q\Omega$. In both equations the scattering angle θ is implicit in both the scattering cross-section σ' and the integration pathlengths. This section treats the separate determination of Ω, Δ and θ, which are (usually) fixed in any one run.

Solid-angle is troublesome to measure accurately at the 1% level, as is routine charge collection in RBS systems, and analysts have used standard (certified) samples for decades to avoid routine use of absolute values of charge and solid-angle. It is difficult to determine the detector-to-target distance with a precision of 1% (generating a 2% uncertainty in the solid angle). It should be noted that if the charge.solid-angle product is calibrated on one beam, then care should be taken that there is no relative error introduced via current integration when performing an experiment in the same geometry with a **different** beam. The comments on solid angle determination apply to particle detectors, where the intrinsic detector efficiency is known to be 100% for energies exceeding ~30 keV. For γ-ray and neutron measurements, it is more difficult to achieve an accuracy of ~1% for the overall detection efficiency.

3.1 Energy

Accelerator energy calibration is critical for accurate work. Clear pitfalls here were highlighted in the last Handbook (see below sect.3.2) which pointed out that the first RBS Round Robin had very disappointing results partly because of very poor energy calibration. For RBS, the spectra have a similar shape for all energies. Of course, the energy loss is sensitive to the beam energy, but is not nearly well enough known for use in energy calibration. In any case the energy loss for any given layer can rarely be measured with a precision exceeding 1%. But since the cross-section is proportional to $1/E^2$, but linear in gain, an energy error will propagate through to errors in the layer thicknesses determined. For EBS (and NRA), there are very often strong resonances which in some circumstances can lead to very large errors consequent on an energy calibration error. PIXE is the one case where energy is a second order effect and one often finds that PIXE labs are rather cavalier about energy calibration. This is a potentially serious pitfall for those labs if they try to do a more complete analysis using simultaneous particle scattering, as is now desirable with the new codes that handle these multiple techniques self-consistently.

One might think that since all accelerators have resistor chains to distribute the terminal potential down the accelerator column through the column current, the terminal potential could be easily determined through Ohm's Law, since the resistors have fixed values. However, these resistors have extraordinarily high values (typically ~10GΩ) and operate at very high voltages (typically ~40keV), and high value high voltage resistors are known to follow Ohm's Law only approximately, and in any case not reproducibly at the sub-1% level.

Therefore it is necessary to calibrate indirectly, using established standards. The two primary accelerator energy calibration points are the $^{27}Al(p,\alpha\gamma)$ at 991.90±0.04 keV and the threshhold of the $^{7}Li(p,n)^{7}Be$ reaction at 1880.60±0.07 keV. These values are taken from the authoritative Marion (1967) and are still the currently accepted values (but note the more precise value from White *et al.,* 1984, for the latter value). The last Handbook had a Table of accelerator calibration energies, but it should be made clear that many of these are for convenience only, are not accepted values, and should not be used in critical work. For example, the last Handbook had a resonance energy of 3036±2 keV for the $^{16}O(\alpha,\alpha)^{16}O$ reaction, but the IAEA recommended evaluated cross-section code SigmaCalc (2009, also see IBANDL, 2009) gives a resonance energy of 3044 keV.

Secondary calibration points can frequently be used to verify the reproducibility of the accelerator energy, usually at a lower precision, and almost always at a lower absolute accuracy. EBS resonances are very convenient for this purpose, especially since there are a number of resonances at high energies and for ^{4}He beams. See Table 4 for suggestions, but note that the energy *positions* of the resonances do not (usually) have an evaluated uncertainty even though the SigmaCalc cross-sections are evaluated. The exception to this is the C(p,p) reaction, where the energy is very well known. The estimated uncertainties are taken from the original cross-section measurements. To use these resonance energies best, considering that the line shapes can be strongly skewed, one of the IBA codes that can handle EBS correctly should be used to fit the spectra obtained. Very high precision can be obtained if the IBA codes are carefully used, even with the very wide resonances.

Table 2: Primary (recommended) accelerator calibration points for protons

(from Marion 1966, except where otherwise stated)

NB: for threshhold reactions the 2003 masses are used (Audi *et al*., 2003), and see the convenient calculator at www.nndc.bnl.gov/qcalc. 1966 and 1984 values are also given for comparison.

Energy keV	Reaction	FWHM keV	Comment
340.46 ± 0.04	^{19}F(p,αγ)^{16}O	2.4	
872.11 ± 0.02	^{19}F(p,αγ)^{16}O	4.7	
991.90 ± 0.04	^{27}Al(p,γ)^{28}Si	0.1	
1747.6 ± 0.9	^{13}C(p,γ)^{14}N	0.8	
1880.60 ± 0.07	^{7}Li(p,n)^{7}Be		Marion, 1966
1880.443 ± 0.020	^{7}Li(p,n)^{7}Be		White *et al*, 1984
1880.356 ± 0.081	^{7}Li(p,n)^{7}Be		
3235.48 ± 0.29	^{13}C(p,n)^{13}N		
4234.43 ± 0.31	^{19}F(p,n)^{19}Ne		
5796.9 ± 3.8	^{27}Al(p,n)^{27}Si		Marion, 1966
5803.73 ± 0.12	^{27}Al(p,n)^{27}Si		White *et al*, 1984
5803.621 ± 0.100	^{27}Al(p,n)^{27}Si		
6460.47 ± 0.15	^{34}S(p,n)^{34}Cl		
7026.56 ± 1.6	^{60}Ni(p,n)^{60}Cu		
9193.85 ± 0.20	^{54}Fe(p,n)^{54}C		
9510.55 ± 1.46	^{58}Ni(p,n)^{58}Cu		
12728 ± 10	^{16}O(p,p)^{16}O	<2	
14233 ± 8	^{12}C(p,p)^{12}C	<1	
14230.75 ± 0.02	^{12}C(p,p)^{12}C	1.2	Huenges *et al*, 1973
19641.9 ± 1.1	^{12}C(p,n)^{12}N		

Table 3: Accelerator calibration points from He threshhold reactions

NB: 2003 masses are used (Audi *et al*., 2003) unless otherwise stated: see the convenient calculator at www.nndc.bnl.gov/qcalc

Energy keV	Reaction	Comment
1436.7 ± 0.5	^{12}C(^{3}He,n)^{14}O	Experimental (two measurements, Marion, 1966)
1437.9 ± 0.6	^{12}C(^{3}He,n)^{14}O	Roush *et al*, 1970
1436.6 ± 0.5	^{12}C (^{3}He,n)^{14}O	Theoretical (Mattauch, 1965)
1435.82 ± 0.14	^{12}C(^{3}He,n)^{14}O	Theoretical
2966.1 ± 1.7	^{6}Li(^{3}He,n)^{8}B	Experimental (one measurement, Marion, 1966)
2965.0 ± 1.5	^{6}Li(^{3}He,n)^{8}B	Theoretical (Mattauch, 1965)
2964.9 ± 1.5	^{6}Li(^{3}He,n)^{8}B	Theoretical
3796.54 ± 0.33	^{16}O(^{3}He,n)^{18}Ne	Theoretical
4380.035 ± 0.612	^{7}Li(α,n)^{10}B	Theoretical
6088.04 ± 0.32	^{14}N(α,n)^{17}F	Theoretical
6620.54 ± 1.6	^{6}Li(α,n)^{8}B	Theoretical
8131.37 ± 0.67	^{15}N(α,n)^{18}F	Theoretical
11337.86 ± 0.65	^{12}C(α,n)^{15}O	Theoretical
15171.49 ± 0.36	^{16}O(α,n)^{19}Ne	Theoretical

Table 4: Secondary energy calibration points based on SigmaCalc v1.6

NB: Uncertainties are derived from the original literature, not from SigmaCalc, and are standard deviations, not FWHM.

Energy keV	Reaction	FWHM keV	Reference
3885 ± 5	$^{16}O(\alpha,\alpha)^{16}O$	2	SigmaCalc (unpublished to date)
4265 ± 5	$^{12}C(\alpha,\alpha)^{12}C$	27	Gurbich (2000)
3470	$^{16}O(p,p)^{16}O$	2	Gurbich (1997)
1483	$^{24}Mg(p,p)^{24}Mg$	0.3	Gurbich & Jeynes (2007)
1748.5	$^{14}N(p,p)^{14}N$	9	Gurbich (2008)
3198	$^{14}N(p,p)^{14}N$	6	Gurbich (2008)
1734 ± 0.2	$^{12}C(p,p)^{12}C$	45	Gurbich (1998)

A competent operator should be able to obtain a terminal voltage calibration at an absolute accuracy better than 0.1%, but this is not so easy, partly because this level of accuracy is never easy to achieve, partly because precision at this level is usually limited by counting statistics (so that significant beam time is required), and partly because such accuracy requires careful attention to the quality of the sample surface used. The aluminium sample should be well polished (shiny) and *clean*, and the lithium sample (which is very reactive) should have a fresh surface prepared each time *in situ* by cutting with a knife under an argon atmosphere. Bear in mind that you only need a 13nm (5μg/cm^2) alumina layer or a 4μg/cm^2 carbon layer to give a 1keV energy loss for protons at 1MeV.

Moreover, many modern accelerators are tandem machines, where a 0.1% uncertainty in the terminal voltage translates into a 0.2% uncertainty in the beam energy. Analysts should not forget that there is also the injection voltage of the ion source into the accelerator, which is a voltage additional to the terminal voltage, so that when the linearity of the accelerator is determined there should always be a zero offset (of the right sign!) equal to the injection voltage. Of course, this ~20kV injection voltage can (and should) be measured directly with readily available instruments.

The good news is that generating voltmeters (the instruments that monitor the terminal voltage) are usually both very stable and astonishingly precise. Modern tandem machines have GVMs that are reproducible and stable over months at the 0.05% level. However, the GVM is a variable capacitance device that uses the induced AC voltage as a monitor for the terminal voltage. The voltage induced on the GVM is directly proportional to its distance from the terminal, and is therefore subject to a temperature coefficient which on the Surrey HVEE 2MV Tandetron is 0.03/°C. For accurate work using energy feedback based on a GVM the accelerator hall temperature must be closely controlled.

3.2 Solid Angle

In this section we consider the determination of solid angle, one of the critical parameters in Eqs.1&2. This is mostly determined indirectly via a standard, and we will consider first NRA standards and then various RBS standards.

Whenever the cross section varies significantly across the finite solid angle of the detector, as is the case for many nuclear reactions, and also with non-Rutherford elastic scattering, care must be used to properly integrate over the solid angle with respect to the angular dependence of the cross section. Care should also be taken (especially for higher energy incident beams which may give

unexpected nuclear neactions) in choosing an aperture which is not only opaque to MeV α particles, but also for more penetrating particles, for example, high energy protons.

If there is an accurately calibrated radioactive source of small area (for example, ^{241}Am), then the solid angle may be determined directly by placing the source at the position of the target. However, it is usually difficult to reduce the uncertainty in positioning the α -source to the desired 1-2% level.

NRA Standards: In discussing reference standards, we are also talking about those nuclear reactions for which the corresponding cross sections are well known at the level of a few percent. To date, probably the most widely used standard for NRA applications has been that for ^{16}O, specifically anodically-grown thin Ta_2O_5 targets on a Ta substrate. The Paris group (Amsel and Samuel, 1967) pioneered their use through the $^{16}O(d,p_1)^{17}O$ reaction at a bombarding energy of 972 keV and a detector angle assumed to be 150° but more likely to be 164°. Here, there is a broad *(*-85 keV) resonance in the reaction cross section. The protons are emitted with an energy of 1.6 MeV, and the cross section has been measured with a precision of ±3%, with a value of 13.3mb/sr by Davies & Norton (1980) and 13.6mb/sr by Lennard *et al* (1989). Seah *et al* (1988) has reported a successful 'round-robin' intercomparison of absolute measurements in different laboratories using this reaction. Gurbich (2004) has recently reported the excitation function for this reaction at 150°.

For those not having access to deuterium beams, substitution of ^{18}O in the electrolyte allows $Ta_2{}^{18}O_5$ targets to be fabricated. The $^{18}O(p,\alpha)^{15}N$ reaction at E = 750 keV could then be used, although the cross section value is not known as well as for the $^{16}O(d,p_1)^{17}O$ reaction (Christensen *et al,* 1990). The $^{16}O(^3He,a)^{15}O$ and $^{16}O(^3He,p)^{18}F$ reactions are also useful, and some cross section values have been reported (Lennard *et al,* 1989; Abel *et al,* 1990). It should be noted that oxygen from a Ta_2O_5 oxide layer will begin dissolving back into the Ta substrate at a temperature of ~700K (Smyth, 1966). Indifference to beam heating of standards is therefore not encouraged.

The cross section for the $^3He(d,p)^4He$ reaction (Q-value 18353 keV) is very well known (±2%) for a centre-of-mass energy of 250 keV (σ_{lab} = 58 mb/sr) (Davies & Norton, 1980; Möller & Besenbacher, 1980). Unfortunately, ^{3}He targets fabricated via ion implantation are sometimes not stable under prolonged ion beam bombardment (Alexander *et al*,1984; Geissel *et al*, 1984).

Hydrogen Isotope Standards: Stable hydride or polymer targets suitable for hydrogen (or deuterium) thin-film standards are still few. There are problems in the preparation of reference targets via ion implantation (current integration, dose uniformity, depth profiles, and stability: see Amsel & Davies, 1983).

Recently Banks *et al* (2004) showed that standard samples could be made from hydrides of Er, and that these were stable to ^{4}He beams, but the samples were both rather rough and rather thick, needing >5MeV ^{4}He to look all through them with ERD. However, an absolute H (and D) content was determined independently of IBA to better than 2%, and ERD & NRA has an uncertainty of 3.3%. Boudreault *et al* (2004b) have shown an interlaboratory reproducibility for H implanted in Si at 2.2% although the expanded uncertainty (k=1) is estimated at 6%

BAM Hydrogen Standard: Reinholz *et al* (2008) have established an a-Si:H certified reference material (CRM) grown by CVD with about 10at% H in an a-Si layer 1-2 μm thick (on Si substrate) with an expanded uncertainty (k=2) in the H content of about 1% (BAM, 2009).

Bi implanted (Harwell) Standard: In 1975 an RBS round-robin experiment was conducted to test whether or not the often claimed ±2% accuracy was actually being achieved. Several Si wafers were implanted at the UK Atomic Energy Agency (UKAEA Harwell) with ~5.10^{15}Bi/cm^2 at an energy of 40 keV, which locates the Bi distribution at a depth of ~20nm. These samples, which became known as the "Harwell Series I" standards, were then partitioned into 1 cm^2 pieces and distributed to ~50 RBS laboratories around the world. The results, reported by Baglin at the 1975 Karlsruhe IBA conference, were disappointing. Even among experienced laboratories, discrepancies of ±20% were common, and some results varied by 50% or more. The individual causes were never fully

resolved, but from the shape of the 1.9 MeV H^+ RBS spectra (which includes the strong 1.6 MeV resonance in Si), Baglin concluded that several laboratories did not even have a correctly calibrated accelerator energy scale.

Subsequently, a collaboration between ion beam groups at Chalk River (Canada), l'Université de Paris, Harwell, and Geel (Belgium) developed several independent methods of calibrating the Bi content of the Harwell standards, eventually obtaining very satisfactory (±2% or better) agreement among the different laboratories (Cohen *et al,* 1983). In the course of these studies, several of the pitfalls noted in this chapter became recognized for the first time. For example, the energy-dependence of the Bi yield was observed to deviate slightly from the expected $1/E^2$ Rutherford law, and this observation led to the recognition of the electron screening correction. Many pitfalls associated with poor Faraday cup techniques were identified and corrected. Also, the problem of charge exchange along the beam line was found to be responsible for significant fluctuations (±4%) in some of the Harwell Series II Bi implantations (Davies *et al,* 1986).

The resulting comparison, with the same Bi-implanted wafer being used in all three laboratories, showed a ±2% agreement, and therefore showed that RBS can achieve the expected absolute accuracy without the use of any calibrated standard. In practice, since the detector solid angle and the scattering angle are difficult quantities to measure accurately, it is simpler to use a previously calibrated standard instead.

Series I wafers have a Bi content of $4.87(\pm0.08).10^{15}$Bi/cm^2 (Wätjen and Bax, 1994). Series II wafers have the same nominal Bi content as Series I, but fluctuations as large as ±4% have been found (as noted above). Hence, whenever greater accuracy is required, one should obtain a wafer that has been cross-calibrated against a Series I standard. These samples may still be available; however they have now been superceded by the a-Si standard which is readily made, and also by the much more accurate Sb implanted standard. Both of these new standards are described below.

BAM/IRMM Sb Standard: Sb implanted samples are available from IRMM, Geel and BAM, Berlin, and are certified at 0.6% (registered as IRMM-302/BAM-L001: Pritzkow *et al*, 2001; Ecker *et al*, 2002). These samples supercede the Bi implant samples, but are used in exactly the same way.

The samples are an implant of Sb into Si with a range of 160nm and a certified Sb fluence of $48.1(\pm0.3).10^{15}$/cm^2 (1σ uncertainty). The Si wafer has a 90nm oxide (of uncertified thickness).

This standard has been used once to date in published work for a traceable RBS analysis of some As implants (Boudreault *et al*, 2004a), and it has also been used recently to validate Si stopping powers (see next section). In both of these applications the Sb standard was transferred through the a-Si substrate yield, and to do this more accurately the Sb standard was amorphized to a depth of 630nm with a cold 500keV Si self-implant of fluence 5.10^{15}/cm^2.

a-Si Standard: There has been useful work on new standard samples, where the measurand is the surface yield of an implanted (amorphized) silicon sample (Lennard *et al* 1999; Bianconi *et al* 2000) This is nearly equivalent to an absolute measurement of the energy loss of ^{4}He in Si if a series of measurements are made at different energies. Konac *et al* (1998) have made direct measurements of the energy loss of ^{4}He in Si (also known as the inelastic electronic energy loss cross-sections or the stopping power) with an uncertainty of about 2% (these important measurements are often referred to in the literature as KKKNS), and Niemann *et al* (1996) have also made measurements of energy loss in Si with an uncertainty approaching 1%. The stopping power function has been systematically extracted using Bayesian methods, with uncertainty estimates, from the measurements of Bianconi+ by Barradas *et al* (2002) .

In the work of Bianconi *et al* labs made absolute measurements of the charge.solid-angle product, at nominally 1% accuracy, and got agreement within the stated error. The traceability of Lennard *et al*'s work is not so easy to establish, but they obtain the same values, and consistency with

KKKNS. The conclusion of all this work is that the measured Si stopping cross-sections have an uncertainty (1σ) of 2%.

We should highlight the fact that the Si stopping powers stored in the SRIM 2003 database (Ziegler, 2004) were recently used to determine the Sb content of an IRMM certified Sb sample (see above) for 1.5MeV He RBS, and it was found that the certified value was obtained within 0.3% (with a 1σ uncertainty of 0.2%) (Barradas *et al.* 2007). This demonstrates that for this He beam energy the SRIM2003 stopping powers for Si are correct to the 1σ uncertainty of the certified sample: 0.6%.

The point to emphasize here is that Bi or Sb implant samples are specific artefacts, but every lab can make its own amorphized Si samples on demand. Secondary standards must be used systematically with the Bi or Sb certified standards, with the associated error and complexity; not so for the amorphized Si. The difficulty with certifying the Bi implants has been in establishing the real variation across the implant batch, but the uniformity and purity of modern production silicon ingots has been established at extraordinary sensitivity and accuracy: modern standard RBS samples can now take advantage of this.

3.3 Electronic Gain Calibration

It is harder than generally supposed to establish the electronics energy calibration (the gain, keV/channel) with an accuracy better than 1%, and it is easy to make errors of 2% and more. Whenever a spectral *area* is being evaluated (Eq.1) only the charge.solid-angle product QΩ is required (this is the case when using the Bi or Sb standards); but, if the a-Si yield (or other stopping power) is being used to calibrate the solid angle, then Eq.2 is invoked, which uses the product QΩΔ, and the gain is *also* required to evaluate the product QΩ needed for interpreting spectral areas. The Si stopping powers have been compared directly with the Sb standard and are therefore very accurately known (for 1.5MeV He): other stopping powers are not usually known to much better than 4%. Nevertheless, it is a bad analytical mistake to omit the determination of one of the local parameters of the analysis because there may be a systematic error in one of the global parameters. After all, the stopping powers of a material are constant, even if they are not known very well, but the analysis is not repeatable if the local parameters are not accurately determined. In this section we therefore dwell on the determination of the important gain parameter Δ at some length.

To determine the gain we must find a sample that has several (at least two!) elements of both high and low Z at the surface. We use a Au/Ni/SiO_2/Si sample (Fig.4) (Jeynes *et al* 1998), where the Au and Ni films are 15 TFU thick and the oxide is 1500 TFU thick: TFU ("thin film units") = 10^{15} atoms/cm^2: see section 7.3. The Ni film is used to wet the oxide for the Au deposition and this sample has excellent long term stability. For this sample, the Si and O "surface" signals are actually buried under the metal layers, and an accurate calibration must take this into account.

This discussion will be in terms of this sample, and the reader can substitute his own favorite calibration sample. As an example of what is possible: in the very careful work of Bianconi *et al* (2000) a 7 point calibration was used, with a Type A estimate of 0.2% uncertainty (see section 5.1) (this estimate is published in Barradas *et al*, 2007). Munnik *et al* (1995) describe stopping power measurements using RBS with an uncertainty on the gain of 0.16%. Gurbich & Jeynes (2007) determined the gain with a Type A uncertainty <0.1%.

To determine the gain we have to identify channel numbers corresponding to well-known energies, and then do a linear correlation to obtain the gain Δ and offset o values: $E_c=\Delta C+o$, that is, the energy E_c is represented by a particular channel C. The surface signal of element E is given by $E_e=k_eE_0$, where E_0 is the incident beam energy, and k_e is the kinematical factor for element E. The kinematical factor is known analytically of course, and depends (fairly weakly at large angles) on the scattering angle θ. Thus, for an accurate gain calibration, both the beam energy and the

scattering angle must be known rather precisely. This discussion ignores the pulse height defect (see below).

Fractional channel numbers To identify the channel numbers the user chooses the signal peak for very thin layers and the signal half height for thick layers. For an accurate gain determination it is essential to find the channels as real numbers, not as integers. The reader may demur here, saying that the detector resolution is (typically) 16 keV and the channel width is only (say) 3 keV/channel, so we are demanding an unphysical precision. But the reader should remember that, firstly, in accurate work you *always* use one or more significant figures than is justified by the intrinsic experimental precision, to avoid rounding errors; and, secondly, some parameters of the data can be established with a precision *much* greater than the nominal system resolution. This latter point is made very strongly by Jeynes & Kimber (1984) who show that the peak of a distribution in an RBS spectrum can be determined with a precision of about 300eV where the detector resolution is 15keV .

It is therefore clear that the best gain determination will not be made unless numerical methods are used to determine real (fractional) channel numbers precisely. This is, incidentally, the only reason for using ADCs at high resolution for collecting relatively low resolution RBS spectra: in Fig.4 we show 512 channel spectra; but we could easily use 4K spectra, in which case integer channel numbers will be at sufficient resolution for determining the gain as precisely as is possible. But standard theory (the Nyquist theorem) says that sampling at greater than 3 times the resolution gains no extra information; so strictly speaking, 4K spectra are a waste of space!

Correlated gain and offset The IBA codes all have facilities for fitting spectra to extract the electronic gain. Of course, it is necessary to determine both the gain and the offset, even though the value of the offset has no importance, and the gain and offset are strongly correlated. Therefore an error in the offset gives a corresponding error in the gain. This is why it is so easy to have large errors in the gain. The fitting used by the codes may not handle this correlation correctly, giving the user a false estimate of the real accuracy.

Detector resolution Fitting codes usually use some sort of chi-squared function to obtain minimum values. Because the positions of edges and peaks can be determined with extraordinary accuracy from RBS spectra, RBS is very sensitive to the effect of the *detector resolution* on the widths of these edges or peaks. Therefore, the analyst often finds that noticeably different results are obtained where the detector resolution is not correctly determined (see §3.6 below).

Pulse height defect Although the machine energy can be established readily at about 0.1%, the absolute electronics calibration depends on an accurate knowledge of the pulse height defect of the detector. Semiconductor radiation detectors are known to respond in a non-linear fashion to particle energy. Normally, the deviations are lumped into the so-called 'pulse height defect' (PHD), which includes the effects of the detector entrance-window and dead-layer, and also the nuclear (non-ionizing) energy loss of the projectile arising from elastic collisions with the atomic lattice of the detector material.

The discussion above ignored this effect, treating the energies of the surface signals as being given only by the kinematics. However, in reality, the detector sees only that fraction of the energy of the particle that is deposited into electron-hole pairs (that is, *after* passing through the entrance window and dead layer), and where the electrons do actually reach the detector anode and are not lost in recombination sites (defects). Old detectors may have significant radiation damage giving a significant number of recombination sites. These detectors will no longer behave linearly, and cannot be used for accurate work, although all the IBA codes allow non-linear gains to be used.

But all detectors, even high quality (new) ones, will detect a particle energy significantly less than the particle has when leaving the sample, due to the PHD. Now usually this can be ignored since the absolute value of the correction is small. For instance, Bianconi's (2000) high precision gain determination referred to above did not correct for the PHD, but this introduces an error of only

0.2% (Barradas *et al*, 2007). Moreover, the non-linearity in the detector response which must exist, since the PHD varies with particle energy, is so small that it cannot be detected in standard cases (Jeynes *et al*, 1998), being mimicked by a (slightly different) linear gain. However, in cases where different spectra collected at significantly different beam energies must be compared, it is essential to do the PHD correction for the best accuracy.

The PHD has been comprehensively described by Lennard *et al* (1990), and Jeynes *et al* (1998) have presented a full (manual) analysis in a particular case where the best demonstrable accuracy for the electronic gain Δ was only 0.5%. Lennard *et al* (1999) do not make a comparable accuracy estimate explicitly, but their work is also consistent with an accuracy in Δ of about 0.5%. The extremely accurate analysis Munnik *et al* (1995) includes a full PHD correction, and Gurbich & Jeynes' (2007) benchmark measurement of the ^{nat}Mg(p,p)^{nat}Mg elastic scattering cross-sections depends on the analysis of a PHD-corrected set of spectra with a single gain across the whole energy range (see Fig.3 for one of these spectra).

There is a further effect that has been studied in some detail (Lennard *et al,* 1986; Bauer & Bortels, 1990; Comedi & Davies, 1991) in Si for light ions (^{1,2}H, ^{3,4}He, ^{7}Li, ...) which arises as a consequence of the differing ionization densities produced by the incident particle. In principle, an IBA spectrum can easily be obtained using higher energy beams for which various nuclear reactions occur and various types of particle all enter the detector; for such a spectrum one could perhaps use a single absolute electronics calibration if the PHD correction could be done correctly. However, no PHD-corrected data has been published for these sorts of NRA spectra that also corrects for the particle type, although Pascual-Izarra & Barradas (2008) describe a full PHD correction in detail..

3.4 Scattering Angle

The scattering angle θ is the angle the detector makes with the incident beam. This should be measured as accurately as possible since even at θ =150° and normal beam incidence an uncertainty of only 0.2° gives an uncertainty of 0.3% in fluence measurements (see section 5). For glancing beam exit geometries any uncertainty in the scattering angle greatly amplifies the uncertainty of the results.

Where a goniometer is used (presumably including most applications of glancing exit geometries) it is easy to measure scattering angle: you only have to shine a laser down the beam path and reflect it onto the detector from a mirror at the sample position. The scattering angle is then read from the goniometer. Care must be taken in precision work to specify the plane of the sample since this affects the scattering angle. For small detectors the blocking effect in single crystals can also be used to detect the scattering angle. In this method you align a major axis of the crystal with the *detector* (not the beam) looking for the dip in yield. The beam energy has to be such that the detector solid angle is not too much larger than the channelling critical angle.

In some cases the angle subtended by the detector has a significant effect on the result. For glancing beam exit work the detector must be collimated in one direction to restrict the possible variation in scattered particle exit pathlength to the detector. For these geometries it is worth noting that *curved* collimation slits are optimal (Brice & Doyle, 1990). For some elastic (non-Rutherford) backscattering (EBS) reactions the cross-section varies strongly (and non-linearly) with scattering angle, and for larger detectors the average scattering angle may not accurately represent the data. This is actually another good way to determine real effective scattering angles. For example, for the 1735keV resonance in the ^{12}C(p,p)^{12}C EBS reaction, the maximum cross-section relative to Rutherford for 150° is 39.06 but for 150.2° it is 39.34, a change of nearly 1%. Conversely, if you are using EBS resonances to analyse light elements you have to verify your actual angles for accurate work.

3.5 Detector Resolution

We have already noted above that fitting programs are sensitive to the value used for detector resolution since the shape of edges and peaks are determined very precisely in RBS spectra. Fig.4 shows a Au/Ni/SiO_2/Si calibration sample spectrum with fits assuming various detector resolutions. The signals from the thin metal surface layers have a shape entirely determined by the detector resolution. To determine the detector resolution you have to match the *height* of the signals, given that the signal *area* is also matched. The fitted gain is given in all cases in Fig.4, given that the metal thickness is fixed. A 4% change in resolution gives a maximum 0.25% change in gain. The fact that the gain can be affected at all by the resolution, albeit at second order, is surprising at first sight.

Also shown is the fitted metal thickness: in this case a 4% change in the resolution gives a 1.5% change in the fitted thickness. This is almost a first order effect even though one might have thought that there should be no change; the size of this sort of effect depends strongly on how the fitting algorithm (in this case a grid-search chi-squared type) works: the reader should be warned that fitting algorithms do not always behave as they intuitively expect.

In principle, the detector resolution function is neither Gaussian nor even symmetrical , and in the most accurate work it is necessary to account for this in detail. This should be done as a matter of course for PIXE, where the detectors are relatively high resolution (typically <200eV) and where the shape of the instrumental function is well known to be non-Gaussian: the GUPIX (see Blaauw *et al.* 2002) program, for instance, assumes that the instrumental function is specified in detail by the user. For PIXE the instrumental function must be measured as a function of X-ray energy over the whole energy range using a series of pure targets. If this is not done the ratios of the various K and L lines cannot be determined with precision. Particle scattering detectors have much lower energy resolution (typically ~15keV), and the instrumental function of these detectors is not usually measured in detail, although remarkable results can be obtained when it is. Fischer *et al* (1997) for example have demonstrated that they can reliably resolve the isotopes of Co using a full Bayesian deconvolution code! However, none of the routine IBA codes currently have facilities for a particle scattering detector resolution that is a function of energy, and the highest resolution work yet reported with these detectors (determining interface roughness of <1nm) used a simple Gaussian (symmetrical) function (Barradas, 2002).

But in general, the lesson is that for accurate work *all* the parameters should be correct.

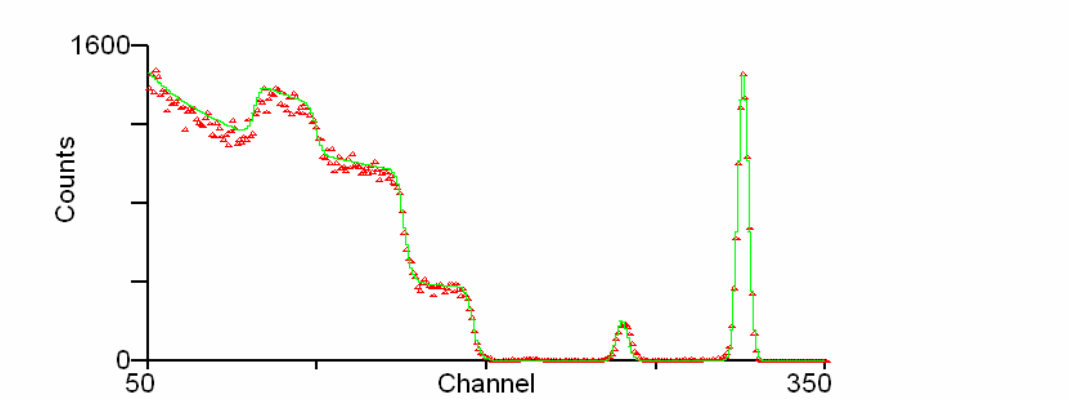

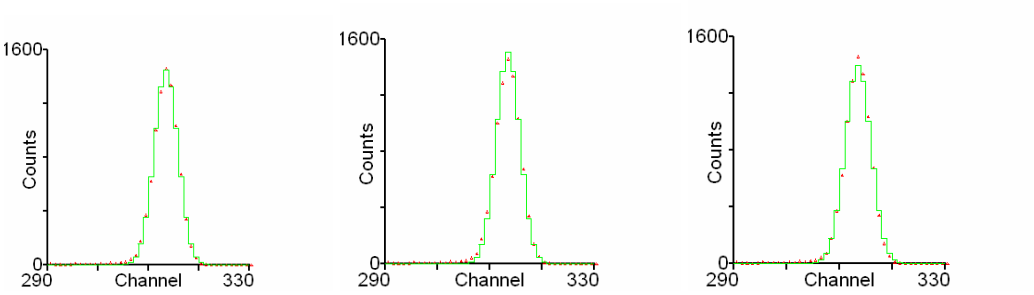

Figure 4: Detector resolution and the effect on calibration of gain. *!.557MeV $^4He^+$ RBS with scattering at 149.2°. Sample is Au/Ni/SiO_2/Si (12.8/14.8/1607 TFU). (a) Detector resolution 25keV, fitted gain for fixed metal thickness 4.457keV/ch,(fitted metal thickness 28.55TFU); (b) 24keV, 4.472keV/ch,(28.07TFU); (c) 26keV, 4.460keV/ch, (28.96TFU)*

4 Algorithmic Issues

In this section we consider a number of effects that affect the interpretation of spectra, and provide occasion for various subtle pitfalls for the unwary. To do an traceable analysis we have to be able to accurately estimate the parameters in Eqs.1 & 2 (considered in turn above), but we have also to be able to accurately do the integrations implicit in these equations. Here we will consider how well known are the Rutherford (and non-Rutherford) elastic scattering cross-sections, and the inelastic electronic stopping cross-sections. We will also discuss the limits within which the basic single scattering assumption is valid, and how well the user can calculate the variation of the energy resolution with depth.

4.1 The Rutherford Cross-Section

How accurate is the Rutherford scattering law? This is often the key question in achieving quantitative RBS analysis, since its main advantage is the assumed existence of a universal and predictable scattering cross section, σ_R (cm^2/sr), whose dependence on beam energy E (MeV), scattering angle θ, and atomic numbers Z_1 and Z_2 of the beam and target atoms, respectively, may be accurately described by Rutherford's formula obtained from the Coulomb potential (see Ch.???).

The validity of this point-charge Rutherford scattering law requires the distance of closest approach (or 'collision diameter'), b(pm)=$1.44Z_1Z_2$/E(keV), between the projectile and target nuclei to fall within the Rutherford 'window' (although, note that this 'window' does not really exist: see Gurbich, 2004). This means that b must be considerably larger than the nuclear radius, r_n(fm)=$1.4A_2^{1/3}$, of the target atom. At the same time, b must also be much smaller than the atomic K-shell radius, r_K(pm)=$50Z_2$, in order to minimize electron screening effects. A quick and simple estimate of the upper and lower energy limits within which the scattering cross section should be within ±4% of the σ_R value may be estimated by requiring $r_K/2>b>3r_n$.

Note, however, that a small screening correction to σ_R is always necessary even though most of the collision is completely unscreened. This arises because the initial part of each scattering trajectory is fully screened (i.e., from ∞ to $50Z_2$ pm from the target nucleus). Consequently, the incident projectile penetrates into the unscreened region with somewhat higher energy than would occur if the target atom was a bare nucleus. The resulting decrease in cross section below σ_R is usually much less than 4%. Furthermore, experimental studies by L'Ecuyer *et al.* (1979), Andersen *et al*. (1980), and Hautala and Luomajarvi (1980) show that its magnitude is predicted (with reasonable accuracy in most cases) by the relationship

$$\sigma = \sigma_R [1 - 0.049\, Z_1\, Z_2^{4/3} / E] \qquad (3)$$

where *E* is the projectile energy in keV. Strictly speaking, the centre-of-mass energy should be inserted in Eq. 3, but the screening correction is usually small enough that the use of laboratory

coordinates introduces negligible error. This L'Ecuyer correction is incorporated in the main IBA codes. The uncertainty in the screening correction is cited as ½% by Wätjen & Bax (1992) for the case of 1.5 MeV ^{4}He on Bi and this uncertainty can be scaled for other cases from Eq.3. However, for small scattering angles, or for heavy ion beams, L'Ecuyer's correction is not as accurate as that proposed by Andersen, which takes into account the dependence of screening on the scattering angle. Andersen's correction is also incorporated in the main IBA codes, and should be used.

If the energy exceeds the upper limit for RBS then we are in the regime of non-Rutherford elastic scattering (EBS). As examples, proton scattering on C is significantly non-Rutherford at 380 keV, and He scattering on C is significantly non-Rutherford at 2.2 MeV. The rough estimates above should not be relied on for accurate work: instead measured cross-sections should always be used. The IAEA has sponsored a database of EBS cross-sections (IBANDL, 2009). The analyst should beware that these cross-sections are a strong function of scattering angle, so that if measurements are not available for the angle used then accurate EBS work cannot be done. However, for some nuclei the EBS cross-sections have been evaluated by A.F.Gurbich, who has determined the quantum mechanical parameters of the nuclear scattering by a fit to all the available data for these nuclei (SigmaCalc, 2009). These cross-sections are the most reliable, and are valid for (almost) all scattering angles. Both the IBANDL database and the SigmaCalc calculator are under active development, and analysts should check whether cross-sections they need are included yet. Where SigmaCalc has cross-sections they should always be used. Note that the IBA codes always give the user access to these cross-sections even if they have default values, and the user should know which cross-sections are being used. Various pitfalls in the use of these cross-sections, which can vary extremely rapidly with energy, are explored in Ch.???.

If the energy is below the lower limit for RBS then the major part of the collision takes place before the projectile has penetrated all the electron shells of the target atom; that is, the unscreened Coulomb field assumed in Rutherford scattering plays a minor part in the collision. With MeV accelerators and surface barrier detectors this almost never happens, even for the heaviest target nuclei. However, backscattering studies in the Medium Energy Ion Scattering (MEIS) regime involve energies well below the limit for Rutherford scattering. For quantitative work, suitable algorithms are given by Mendenhall and Weller (1991); however, they point out that a fairly accurate (2-3%) approximation to the screened Coulomb cross section can still be obtained by applying the simple screening correction of Eq.3.

4.2 Electronic Stopping Cross-Sections

Almost all IBA work relies on electronic stopping cross-sections. In particular, quantification of depth profiles depends on the stopping power values used. The same is true of elemental concentrations in most cases.

There are different sources of stopping powers available, from *ab initio* theoretical calculations to experimental data covering a limited energy range of a given ion in a given material. The most widely used source is SRIM (Ziegler, 2004), which is a semi-empirical interpolation scheme, that covers all ions at all energies in all materials. Users should be aware that SRIM has evolved over the years, and different versions provide different stopping values. The same is true of data analysis codes, where different versions may incorporate different SRIM versions. Other sources of tabulated stopping powers exist and are also used, namely ICRU (1993) and MSTAR (Paul & Schinner, 2001, 2002) (the latter for heavy ions only).

A statistical analysis made by Ziegler, including all the over 25000 data points in the SRIM2003 data base, shows that the accuracy of SRIM2003 stopping calculations is 4.2% and 4.1% for H and He ions, respectively. The accuracy is only 5.1% and 6.1% for Li and heavier ions, respectively. However, these numbers are average estimates, and do not represent the uncertainty for any given system. In the same analysis it is shown that SRIM2003 predicts around 75% of stopping values within 5% of experimental values for H and He ions, but only 58% for heavy ions. That is, for

heavy ions 42% of stopping power values calculated with SRIM2003 are off the experimental ones by more than 5%. This decreases to 18% for errors larger than 10%. It is worth noting that the experimental measurements are notoriously hard to make, so that even if SRIM reproduces the experimental data there is no guarantee that the data are correct.

The outcome is that for H and He ions (and increasingly for Li as well), the tabulated stopping values are normally accurate (at the 5% level), but in some particular systems large errors can be made. Users interested in high accuracy should check the literature for experimental values, and compare them with the calculations. In some systems, highly accurate data are available. On the other hand, for heavier ions, the experimental data are sparse, and the calculations can be inaccurate for many systems. Advances in the accuracy of heavy ion stopping are being continuously made, so the situation may improve in the coming years. In the meantime, reliance on tabulated, often interpolated, stopping values may be the only practical solution, but it can lead to large errors.

Paul and Schinner (2003, 2006) conducted statistical analyses of the accuracy stopping powers from different sources, including SRIM2003 (and older versions of SRIM), ICRU, and MSTAR, for light and heavy ions in solids, gases, and compounds. The main conclusion is that the three sources are equally accurate in most cases, as long as the most recent versions are used.

Great care should be exercised when analysing compounds, particularly insulators, since most codes use the Bragg rule to calculate the compound stopping from the elemental stopping powers. This approach leads often to larger errors. SRIM2003 implements the so-called cores and bonds (CAB) correction, which is however limited to some tabulated compounds. The alternative is to use the molecular stopping powers if available from experiments, which some IBA codes can use.

In all cases we should emphasise that when using Eq.2 the dominant uncertainty almost always comes from the stopping power database.

4.3 Plural and Multiple Scattering

One major assumption in most RBS and IBA studies, is that the incoming and outgoing trajectories are completely linear, that is, only one significant angular deflection, namely the Rutherford backscattering event, is occurring. However, the mean free path for unscreened scattering events $[(N.\pi.\ a_{TF})^{-1}]$ is only ≈100nm, where N (atoms/cc) is the atom density of the target and a_{TF} ≈10pm is the appropriate Thomas-Fermi screening length (and note that at MeV energies, only unscreened scattering can contribute significantly to the mean deflection angle). Hence, even at quite shallow depths, a fraction of the beam undergoes significant secondary deflections along the incoming/outgoing trajectories. If not accounted for, these can lead to wrong interpretation of data.

Full quantitative treatment of such effects require a Monte Carlo simulation of each particle trajectory. Major improvements in the accuracy and efficiency of such calculations were obtained (Arstila *et al.* 2001), but they are still difficult to use in routine work. Some traditional codes now include both multiple and double scattering.

The term plural scattering describes trajectories where the ion suffers several large angle scattering events before being detected. A particular case is double scattering, corresponding to two large angle events. The combined kinematic factor can be larger than the kinematic factor for single scattering, leading to yield *above* the nominal surface signal energy. The most important effect is however an increase of the yield at low energies, and a low energy background.

At least two well-known data analysis codes, SIMNRA (Eckstein & Mayer, 1999) and DataFurnace (Barradas, 2004), include the calculation of double scattering in RBS, as a user option. Calculation times are much longer than for single scattering. One example is shown in fig. 5, where the SIMNRA simulation matches both the data and a Monte Carlo simulation for 0.5 MeV ^{4}He ions backscattered from about 115 nm Au on Si at a scattering angle of 165°. A comparable RBS example for DataFurnace shows a TiAlN/Mo multilayer measured at grazing incidence, with a

good fit including the effects of a large double scattering signal extending to low energies (Barradas & Jeynes, 2008).

Multiple scattering refers to the succession of many small angle scattering events, leading to an angular broadening in the beam path. Such secondary deflections obviously change the scattering angle involved in the main RBS collision thus affecting the magnitudes of both the cross section and the kinematic energy loss factor. Furthermore, it also affects the depth-to-energy conversion scale.

However, the net effect of multiple scattering is, in first order, an extra contribution to the energy spread of the beam (Szilágyi *et al*, 1995). This can be the largest contribution to straggling in some situations, particularly in grazing angle experiments, and must be taken into account for a correct interpretation of the data.

A second effect of multiple scattering is that the shape of the energy spread is no longer Gaussian. This can become important for heavy ions in heavy targets, at low and intermediate energies. Some limited treatment of this is included in some IBA codes.

Multiple scattering is very small for light ions at near normal incidence (and detection). It can be very large for heavy ions, or for grazing angle incidence or detection even for He beams. In that case, whenever depth profiles, roughness, or other sample features that affect the sharpness of signals are studied, the contribution of multiple scattering to straggling must be calculated and included in the analysis.

Note that current versions of a popular computer code for simulation of RBS profiles, RUMP (Doolittle, 1985, 1986), do not include any treatment of plural or multiple scattering.

4.4 Depth Resolution

Depth resolution is defined as the minimum separation in depth between two layers, such that to each layer a maximum in the observed signal is observed. It determines the capability to separate signals from different layers.

Depth resolution is best near the surface, and degrades due to energy straggling in deeper layers. There are different contributions to depth resolution: the detection system resolution, energy loss straggling, multiple scattering, beam energy and angular spread, finite size of the beam spot on the sample, and finite size of the detector. The last three terms together are usually called geometrical straggling and influence the energy resolution because they lead to a spread of possible beam trajectories. The code DEPTH (Szilágyi *et al*. 1995**Error! Bookmark not defined.**) uses state-of-the-art theory to calculate the different contributions. Given that there are very few energy spread measurements available, it is currently the most reliable source for depth resolution. SIMNRA implements the same straggling calculations independently.

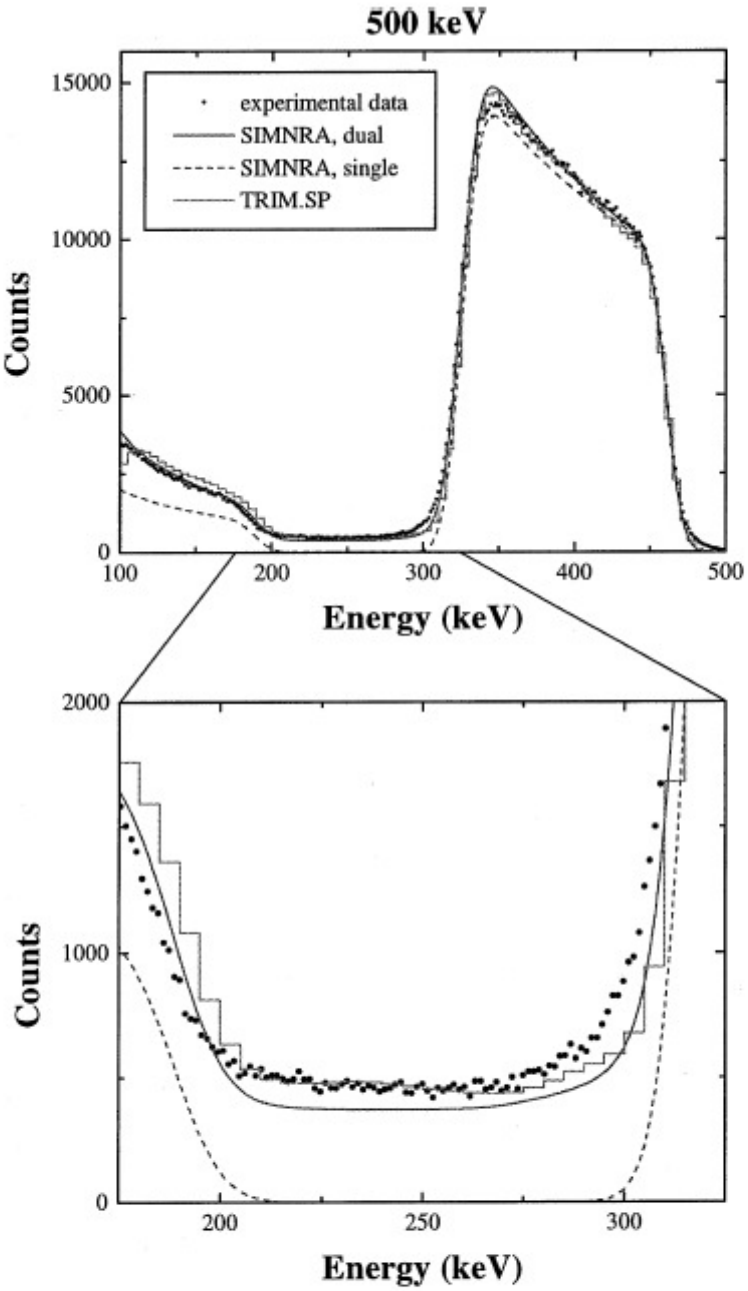

Figure 5: Double scattering effects in ^{4}He RBS of Au on Si

Comparison of the experimental energy spectrum (dots) at a polar emission angle of 15° for 0.5 MeV ^{4}He. The histogram gives the TRIM.SP result; the dashed line represents the single collision model and the solid line the dual collision approximation, both calculated with SIMNRA. The lower part of the figure shows the background between the Si edge and the lower Au edge in more detail (reproduced from Eckstein & Mayer, 1999)

Different pitfalls often arise when depth resolution is not well understood .If the energy spread at a given depth is not well calculated (for instance due to neglect of multiple scattering or geometrical broadening), then the simulation for sharp interfaces will be sharper than the observed data; the user may then wrongly conclude that the sample has strong interdiffusion between layers or rough interfaces.

Analysts can also be tempted to retrieve more information than the data justifies. This is normally done by imposing their favourite model on the data, without testing other possibilities that could also lead to a good fit within the depth resolution at a given depth. In this respect, over-reliance on

e.g. χ^2 goodness-of-fit can lead to ultimately wrong data interpretation, because, as seen in section 3.7 above, the depth resolution used directly affects the results.

5 Accurate IBA

The ultimate consideration of all analysis is the accuracy available. We use accuracy here in the critical sense, that is where a measurement can be traced back to international standards of mass, length and time with a specifiable uncertainty. Because the Rutherford cross-section is analytical the accuracy of RBS is potentially unlimited—except for the major problem in all IBA, the limited knowledge of the energy loss of ions in matter that we considered above (Section 4.2). However, there are certain sorts of analysis where the energy loss enters only in second order: one of these cases has been treated in detail by Jeynes *et al* (1997) with the conclusion that even in this ideal case there are several small effects that have to be considered (at the ¼% level) that will cumulatively make an accuracy better than 1% hard to acheive. (We quote all uncertainties here at the 1σ confidence level.)

The only doubt about the potential accuracy of RBS to our knowledge is the interpretation of the low energy tails in backscattering spectra. Tails are certainly caused by multiple and plural scattering effects and have been calculated successfully with Monte Carlo techniques by Bauer *et al* (1992, 1993), and by Eckstein & Mayer (1999) for low energy beams where the effects are large. They could also be caused both by slit scattering and any low energy component there may be in the beam. However, it has been claimed by Gurbich (1995) using time of flight techniques with a 2MeV pulsed proton beam and very thin (10keV) self-supporting gold foils, that the low energy background cannot be explained by plural, multiple, and slit scattering alone, which would mean that some significant physical phenomenon is still left unaccounted. In any case, the single scattering approximation certainly fails sometimes: Barradas *et al* (2007) have pointed out that the calculation of some heavy ion ERD spectra by the IBA codes is not consistent with a Monte Carlo calculation: however, it is not yet known absolutely how reliably these agree with experiment. Gurbich also does not give sufficient detail of his MC calculation to evaluate his result.

In this section we consider a systematic approach to the estimation of uncertainty, including a discussion of the explicit uncertainty budget that must be included in any standards work that claims to be traceable to international standards. An important benefit of IBA, and the focus of this chapter, is the availability of absolute accuracy, but no analysis has any value unless the analyst is able to reliably specify its uncertainty.

We also have an extended discussion of analytical approaches to the recognition and avoidance of ambiguity in IBA data. It is of great importance for the analyst to recognise the difference between *necessary* conclusions (*required* by the data) and *valid* ones (*permitted* by the data). In many materials problems that IBA is applied to, the user will want clear-cut answers from the analyst. The analyst therefore needs to gain skill in seeing objectively what information is really contained in the data, and how to apply prior information from the user to eliminate various valid solutions of the data.

5.1 Uncertainty Estimation

TypeA & TypeB We start by referring the reader to the *Guide to the Expression of Uncertainty in Measurement* (GUM, 1995). According to GUM, there are two types of uncertainty estimation: Type A and Type B. Uncertainties are type A when they can be calculated as a standard error from a set of measurements. They are type B when the statistical data needed for type A is not available, and the user has to make a more informal estimate of the probable measurement error. So for example, a measurement of length may be made with a ruler. The experimenter could estimate the uncertainty of a single measurement by assuming a maximum reading error of say half a graduation. This would be a Type B estimate. On the other hand, to get a Type A estimate he could make a

series of measurements, and then take an average and a standard deviation. It is worth noting that Type A estimates are not always better than Type B estimates. In the case of a ruler measurement for example, there may well be a systematic reading bias from an observer, which may go unnoticed. This is not such a trivial point as it seems. Polanyi (1958) rehearses the famous case

> … of the Astronomer Royal, [Nevil] Maskeleyne, who dismissed his assistant [David] Kinnebrook [in 1796] for persistently recording the passage of stars more than half a second later than he, his superior. Maskeleyne did not realize that an equally watchful observer may register systematically different times by the method employed by him; it was only Bessel's realization of this possibility which 20 years later [after considerable work by Bessel, who was the first, in 1838, to observe stellar parallax] resolved the discrepancy and belatedly justified Kinnebrook.

Table 5: Uncertainty Budget

coverage factor k=1

(Reproduced from Jeynes et al 2006)

	Type A or B	IBM detector	Cornell detector	Comment
Pileup correction		2.60%	0.80%	
Uncertainty of pileup correction	A	2%	2%	From shape fitting accuracy
Counting statistics, As signal	A	0.28%	0.47%	
Counting statistics, a-Si signal	A	0.08%	0.13%	
Scattering angle	B	0.28%	0.07%	0.2º and ~$1/\sin^4\theta/2$
Electronic gain	B	0.5%	0.5%	
Pileup correction	A	0.05%	0.02%	See separate section above
Relative uncertainty		0.64%	0.70%	
Relative uncertainty of average of two detectors		0.48%		average / √2
Beam energy	B	0.20%		These are the same for both detectors
Rutherford cross-section	B	0.16%		Screening correction
Combined standard uncertainty		0.54%		Relative accuracy
IBA code uncertainty	B	0.2%		From software intercomparison (Barradas *et al* 2007) For HI-RBS this value is 0.7%, for He-ERD this value is 0.4%
Si stopping power	B	0.6%		From software intercomparison (Barradas *et al* 2007) since SRIM 2003 stopping powers were used
Total combined standard uncertainty		0.83%		Absolute accuracy

We note further that GUM speaks of "***uncertainty***" (indicating that our knowledge is limited) rather than "***error***" (which implies that a mistake has been made). It also uses the idea of "***coverage***", so that, instead of saying "the 1σ error was 2%", GUM uses the more generalised terminology "the

expanded uncertainty was 2% with a coverage factor k=1". Of course, in all cases both TypeA and TypeB uncertainties must be estimated, and combined as necessary.

Uncertainty budget The "uncertainty budget" is specified by GUM as a formal approach to the systematic evaluation of the uncertainty of a measurement, which is essential when a critical result is presented the traceability of which must be explicit. This has been described with special reference to IBA by Wätjen and coworkers (Sjöland *et al.* 2000). We emphasise again that IBA is a quantitative analytical technique which is capable of great precision and whose uncertainties are well-known; we do our users a disservice by not properly estimating these uncertainties.

The uncertainty budget for the analysis of Fig.1 is presented in Table 5 as an example. All the sources of uncertainty are listed, making the origin of the claimed combined standard uncertainty very clear, and hence easy to evaluate critically. It is clear that the stopping power uncertainty dominates the total combined uncertainty.

It is this sort of treatment that is able to establish the traceability of a measurement, and thus justify the weight that is put upon it. We note that IBA is very simple, and specifying its traceability to international standards of weights and measures is relatively easy. The present treatment is a significant simplification of the GUM recommendations, which can be applied successfully to much more complicated cases.

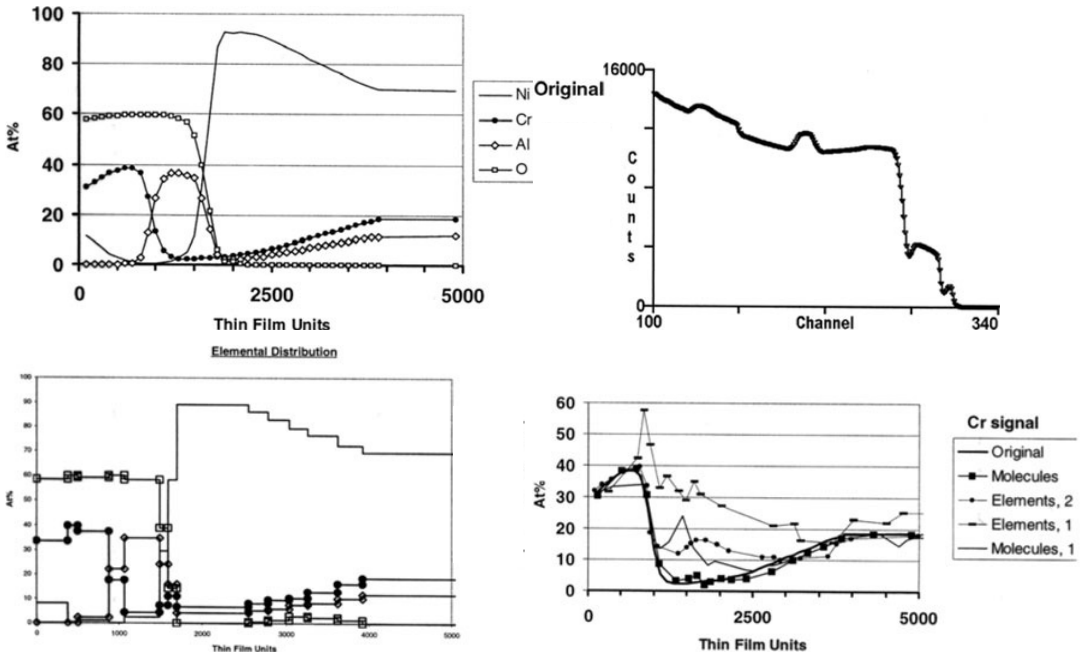

Figure 6: Butler's (1990) example of an oxidized NiCrAl alloy re-analysed (reproduced from Jeynes et al, 2002) (a) The original profile from which the spectrum was calculated; (b) spectrum (symbols) and fit (line); (c) atomic profile fitted to data assuming molecules and complete oxidation from the surface, using two spectra at different detector angles, and excluding alumina from the surface; (d) a comparison with the original profile of the Cr profile calculated under various assumptions. Specifying only elements barely constrains the profile, and even with two detectors the profile is not recovered at intermediate depths. Using only one detector with the assumption of molecules is also not sufficient. Molecules used are NiO, Cr_2O_3, Al_2O_3 and $Ni_{195}\,Cr_{186}\,Al_{119}$.

5.2 Spectral Ambiguity

In this section we follow the treatment of Jeynes *et* al (2003) which also has further examples. We will show that IBA spectra are grossly ambiguous in general, and we will re-analyse the ambiguous spectrum previously discussed masterfully by Butler in 1990. There are two approaches to overcoming this ambiguity: the first is to collect multiple spectra under different conditions to constrain the solutions found (where a "solution" is an elemental depth profile which has a spectrum that fits the data), and the second is to rule out *a priori* certain types of solution, which we will

call "restricting the state space", where the state space is the multidimensional space containing all possible depth profiles.

We say that an optimal solution is a depth profile from which a spectrum can be calculated that fits the data well, and that a spectrum is ambiguous where more than one optimal solutions exist.

For the As implant of Fig.1 for example, one element in the state space is a pure As sample, another is a pure Si sample, and there are a very large number of intermediate elements. The state space is large, but it is not infinite since the energy resolution limits the number of layers that must be considered, and the detection sensitivity limits the number of layer compositions that must be considered.

Multiple spectra: Every analyst has tilted the sample and taken another spectrum to determine which features of the spectrum come from the surface: the *surface* signal position does not vary with beam incident angle, although signals from below the surface will appear to move as the geometry changes. An equivalent way of doing this is to use two detectors at different scattering angles. This is not a new idea: Williams & Möller were using two (or more) detectors in 1978 (although with a rather different purpose) and Edge (1988) showed calculations emphasising the value of spectra from two detectors, but using an iterative method of calculation not easy to extend to three or more spectra. Butler (1990) emphasises the value of multiple detectors and Alkemade *et al* (1990) demonstrate that for a sample with n elements, one needs in principle to collect n-1 different spectra to eliminate ambiguity.

Fig.1d shows an example of the independently collected data from two detectors directly compared: in this case exactly the same quantity (the depth profile of As) is measured by each detector, and the profiles should overlap. That they do is an indication that the independently determined electronic gain calibrations are reliable. The FWHM of the As signals are different since the detector energy resolutions are different. The signals at negative depths are because the channel data is being replotted directly on a depth scale, without correction for broadening due to the detector resolution and straggle.

Restricting the state space: It is very easy to demonstrate that RBS spectra are ambiguous. Butler showed an example which is ambiguous in the sense that different depth profiles exist where different partial spectra add up to the same total spectrum: we discuss this interesting case below. However, we have not (yet) found any examples where IBA data are systematically ambiguous in the sense that the system is "frustrated" in Kirkpatrick *et al*'s (1983) terminology; that is, where a number of optimal solutions exist between which are large potential barriers. Other systems are easy to find which are "frustrated": see the related discussion of ellipsometry data by Barradas & Keddie (1999b) as an example

When interpreting such data as the As implants described above (Fig.1) analysts are used to tacitly ruling out the possibility of As deep in the sample because they know that in this case the substrate is pure silicon. However, Barradas *et al* (1999a, "BJJM") have demonstrated that the *most probable* solution of this type of spectrum, assuming that there is some oxygen signal and that there is *no* prior information, is that there is a significant quantity of the heavy element in the substrate. This is because any particular spectrum can be reproduced by many mixtures of the three elements, given that the sensitivity to the light element is limited and there is always some uncertainty about the collected charge.

It is important to be objective about what we know about the sample *a priori*. If we assume *nothing* about the sample then we have to give a range of possible solutions, consistent with the data. Interestingly, BJJM also demonstrated that provided the state space is suitably restricted the RBS data are remarkably *un*ambiguous with respect to collected charge (total number of counts). It is a common pitfall for analysts to collect large amounts of charge to get "smooth" data, but very small charges (BJJM consider 0.1μC with 2.5msr detector solid angle) can give objectively quite well-determined solutions even for "hard" cases, with the right number of layers and qualitatively the

right stoichiometry in the layers. Of course, with less counts in the spectrum the statistical uncertainty of the fitted stoichiometry and thickness of the layers increase as expected. It is worth pointing out that this emphasises the value of backscattering spectra collected simultaneously with microbeam PIXE spectra: microbeams typically use only 100pA, and total collected charge is often a small fraction of a μC. Do not fall into the related pitfall of neglecting the potentially large amount of information in a noisy spectrum!

Butler's example re-analysed: We show Butler's example of an oxidised NiCrAl alloy in Fig.6. He points out that for this example the false solutions can be eliminated if prior *chemical* information is taken into account. Thus, he knows that the oxygen comes from the oxidising process, and therefore enters through the surface. (Actually, most of his false solutions are eliminated simply by excluding O from the substrate.) Moreover, the O binds with the metals in well known ways. Therefore the ambiguity is greatly reduced if the analyst can manipulate *molecular* (rather than *atomic*) depth profiles.

Fig.6a shows the elemental depth profile of Butler's example with a spectrum calculated from it (Fig.6b). Fig.6c shows the solution obtained closest to the original profile, and we discuss this result further below. We point out here that this result is essentially identical to the original, except for some interface broadening (we have not deconvoluted the straggle).

It turns out that the Cr profile is the most sensitive to the prior assumptions of the analysis, and Fig.6d shows the Cr profiles obtained under four different assumptions. To retrieve Butler's initial profile unambiguously we need to specify not only the molecules present but also that *only* oxides are present near the surface *and* that oxygen is excluded from the substrate *and* that Al is excluded from the near surface region *and* that two independent spectra are taken (at different scattering angles in our example). Butler did not point out this last condition for this example, although he noted that, in general, multiple spectra are always a help. These particular data are very ambiguous: many different solutions, all of them as good as that shown in Fig.6b, can be obtained without any of the conditions mentioned.

In this example we have only allowed the O to exist bound to metals, and we have only allowed free Ni to exist. The substrate is specified by a molecule representing the starting alloy composition. It is easy to specify various assumptions about the chemistry to see whether they are consistent with the data. If they are *not* consistent they can be ruled out. Thus, RBS is an effective tool not just for obtaining *a* solution to a spectrum, but for testing a variety of assumptions about the sample against the data.

5.3 Model-Free Analysis and Occam's Razor

In the presence of ambiguity, the analyst must be careful to control his assumptions. The philosophical maxim of William of Ockham from the 14th century known as "Occam's Razor"[1] should be kept in mind by all analysts.

There are many alternative ways to fit any given set of data. If you have found a good fit to the data you may have a *valid* solution. Whether or not it is valid depends on whether you have used correct parameters. Sometimes this may be an intricate question if you are interpreting the detail of a spectrum. Even if your solution is valid, in the presence of ambiguity it is not necessarily *true*. Even if the solution is not false, it may not be *useful* in the case where Occam's Razor has not been wielded. In Butler's example, the spectrum allows one to validly infer a variety of Cr profiles: discriminating between these profiles to determine the real one can be done only if we restrict the number of the parameters of the system (using Occam's Razor), for example, imposing on the system prior chemical assumptions. In this example four molecules are used instead of four

---

[1] Given variously as: *Pluralitas non est ponenda sine neccesitate* (plurality should not be posited without necessity) or: *Non sunt multiplicanda entia praeter necessitatem* (entities are not to be multiplied except of necessity)

elements, but the light element is *correlated* with the heavy elements so that not only is the *number* of stoichiometric possibilities reduced but also the *insensitivity* of the system to the light elements is not allowed to seriously distort the results.

Also, analysts sometimes overlook assumptions they tacitly impose on data when they interpret them according to a model. For example, the As implant profile of Fig.1 could be fitted with a Gaussian distribution, and many IBA codes facilitate this. Now there is nothing wrong with this, so long as it is borne in mind that this is an explicit assumption *imposed* on the data, which can lead to error (which may be large) if the profile is not in fact Gaussian. A model-free fit, imposing no prior assumption on the data, would be with a number of layers of varying stoichiometry. Occam's Razor requires that we restrict the number of layers to restrict the number of fitting parameters. Then there is an explicit tradeoff between the goodness of fit and the number of layers. Clearly, for any given spectrum the number of fitting layers can be increased uselessly to follow the statistical variation of the spectrum. This underlines the value both of Occam's Razor, which highlights and deprecates this uselessness, and of multiple spectra, which will have independent statistical variation and thus naturally discourages too many layers.

5.4 Common pitfalls in data analysis

Here we are concerned with some of the problems and issues that are particularly relevant to data analysis. Many prior assumptions are made in all data analysis, some explicitly, and other implicitly. They all have the potential, if incorrect, to lead to severely wrong results. We can divide the assumptions very roughly in four categories: sample; experimental parameters; physics; databases.

Assumptions on the *sample* include the elements present; a given depth profile or elemental distribution; the existence of roughness, inclusions, and other inhomogeneities. The experimental *parameters* are known with an accuracy, which varies widely for different set-ups. The user may be aware of this accuracy (for instance, a 1 keV beam energy spread), or not (for instance, a 5 keV energy drift with accelerator temperature during an experiment). Assumptions on the *physics* involved include both the analysing beam-sample and the detected particle-detection system interactions. The user can include only the basic physics given in section 3.3, in situations where some of the phenomena described in section 3.4 play a vital role. Using a given *stopping* or *scattering cross section* is an implicit assumption that the data base used is correct for that case. The prior assumptions are often connected to each other. For instance, the assumption on scattering angle implies a consistent assumption on the scattering cross section.

We list in Table 6 the consequences for data analysis of some of the problems that commonly happen due to wrong assumptions, and what can be done to prevent or remedy them. These preventive and corrective actions can be divided into four main groups: *first* and foremost, the knowledge about the set-up used and its characteristics should be as complete and accurate as possible. This often involves elaborate experiments or even the installation of new hardware (for instance to measure the beam charge), and is generally not feasible in the short run. *Second*, alternative experiments, using different beams, energies, and other parameters, or even completely different techniques, may be required - further beam time, or other techniques, are however not always available. *Third*, programs that include the best physical models and data bases available for the problem at hand should be used. This is often the only practical alternative for the data analyst, who is thus often confronted with problematic data.

Table 6: Pitfalls and remedies in data analysis

Caution should be used where the suggestion is to treat as a fit parameter: this may lead to even larger errors!

Assumption on	*What went wrong*	*Consequences*	*What can be done*
elements present	impurities are ignored	impurity signal wrongly assigned to some other element (possibly one with small cross section leading to large consequences on the overall solution)	use complementary technique that can detect the impurities; link the impurity to a major element
	a "missing element" is falsely postulated or ignored	wrong fitted charge to accommodate the unobserved element, with consequences to all other elements	use complementary technique that can detect the missing element; or collect spectra in different experimental conditions
depth profile	false depth profile was chosen, leading nevertheless to a good fit (IBA is often ambiguous)	results are all wrong	collect spectra in different experimental conditions; test different models
	profile function (such as Gaussian) imposed on some element when real profile is different	results are inaccurate for that element; if signal is superimposed to other fast-changing signals, other elements may be affected	make a model-free analysis; test different models
	sample roughness ignored (often the case in interdiffusion studies)	depth profile retrieved too broad, or completely wrong in severe cases	measure roughness; make grazing angle experiments
	wrong type of sample roughness considered	roughness parameters derived meaningless	determine roughness type; include it in analysis if possible; test different models
beam energy	calibration of accelerator inaccurate	systematic error in analysis, (for RBS this may be partially compensated by MCA calibration and stopping) . EBS cross sections wrong, depth scales wrong	calibrate the accelerator energy!
	energy drifted during the experiment	apparent energy resolution worse than expected, apparent gain changes; cross sections change slightly leading to inaccuracy in the quantification	measure energy drift by collecting calibration spectra at the beginning and end of each run. Discard badly affected data
scattering angle	poor original measurement; problem with moving detector	can give completely wrong results; near-normal incidence and grazing angle experiments become inconsistent	determine accurately the scattering angle (may be difficult); treat as fit parameter
angle of incidence	poor alignment of sample holder; problem with goniometer	can give completely wrong results; near-normal incidence and grazing angle experiments become inconsistent	align sample holder (may be difficult); treat as fit parameter
energy resolution	not determined recently	leads to small error in results; may be crucial if interdiffusion or roughness are important	determine energy resolution in each run; treat as fit parameter

solid angle	not well determined; may change with sample distance	normally assigned to collected charge, leading to an extra error in the results	determine accurately (may be difficult); adjust for sample distance
beam charge	not well determined (or not measured)	not very important if the spectrum has some signal (normally substrate) that can serve as internal calibration. May lead to completely wrong results otherwise	determine accurately (may be difficult or impossible); rely on internal normalization (may be difficult or impossible); treat as fit parameter
stopping power	database inaccurate	elemental concentration and layer thickness values become inaccurate; may lead to completely wrong analysis in severe cases	use a better database if available; determine the relevant stopping powers if possible; make experiment with different beam; treat as fit parameter
	Bragg rule for molecular stopping inaccurate	elemental concentration and layer thickness values become inaccurate; may lead to completely wrong analysis in severe cases	use molecular stopping powers if available; determine them if possible; experiment with different beam is unlikely to help
scattering cross section	required non-Rutherford (EBS or NRA) cross section may not be measured or determined yet, or may be inaccurate	elemental concentration values become inaccurate; may lead to completely wrong analysis in severe cases	determine the relevant cross section; ignore in the analysis the element involved; make experiment with different beam/energy
	calculate cross section for an EBS (or NRA) resonance at a given depth for the average beam energy at that depth	elemental concentration and depth profile of affected element become inaccurate; may lead to completely wrong analysis in severe cases	use codes that correctly integrate cross section over the entire energy distribution of the analysing beam before scattering
straggling	used Bohr straggling where Bohr model is not valid	Diffusion, mixing and roughness results wrong	always use best models available
	did not include Tschalär effect	Diffusion, mixing and roughness results wrong for depths where energy loss is 10-20% larger than initial beam energy	always use best models available
plural scattering	ignored when relevant	introduce (heavy) elements at depths where they do not exist	use best models available whenever plural scattering is relevant
multiple scattering	ignored when relevant	Diffusion, mixing and roughness results wrong	use best models available whenever multiple scattering is relevant
	not well calculated, particularly at grazing angles	results can be wrong	Monte Carlo techniques may be only available alternative; make experiment with different beam
channelling	unnoticed accidental channelling overlooked in analysis	results can be wrong; but if only the substrate signal is affected there may be no consequences unless the substrate signal is used for normalisation	adjust incidence angle, or rotate sample while measuring; calculate channelling
pulse pile-up	ignored when relevant	introduce (heavy) elements at depths where they do not exist; affects signal heights and areas, can dramatically degrade accuracy,	accurate models exist, use them!
Poorly fitted data	could not find correct model	results can be entirely wrong	reliable analysis required well fitted data.

This leads to the *fourth* and most important group of preventive actions, which is to avoid both over-interpretation and under-interpretation of the data. Over-interpretation occurs whenever the data analyst unjustifiably imposes a given model on the data. This often leads to tuning the experimental parameters beyond their known accuracy (such as increasing the charge while scaling the stopping power for a given element in a given layer). The user must consider different models that might lead to an equivalent or better solution. Of course, the *prior assumptions* discussed above (sections 5.2 & 5.3) that the analyst can impose on data to exclude certain valid solutions are also strictly *over-interpretations*, but in this case they are explicitly justified.

Under-interpretation occurs when the analyst does not extract all the information that is actually present in the data. For instance, signal widths, which are often disregarded, have information on both intermixing and roughness. The analyst may not be interested in that further information, but often it is simply due to lack of knowledge (for instance, that new generation codes can extract roughness information with considerable ease). However, most often under-interpretation happens when the data is not well fitted. Modern codes are now available which facilitate excellently fitted spectra, enabling the analyst to put much greater weight on the results.

As a general rule, it is always desirable to collect multiple spectra from the same sample. This can be with multiple detectors installed in the experimental chamber, or by doing different experiments including different techniques. While in simple cases this is not necessary, to analyse meaningfully complex samples multiple spectra and multiple techniques are almost always necessary. The typical example is to use RBS, EBS, ERDA and PIXE to be sensitive to the heavy elements, to specific light elements, hydrogen, and minor contaminants. All spectra collected should be analysed simultaneously with the same depth profile, to ensure a self-consistent analysis.

A major pitfall is the use of the wrong charge.solid-angle product $Q\Omega$ where normalisation of this quantity is not easily available from the spectrum. $Q\Omega$ is implicitly determined by the composition of the sample (where there is no channelling), so that if the wrong value is imposed on the data the results can be severely distorted. An illuminating example of a case where the uniqueness of $Q\Omega$ is used to determine the sample composition with great delicacy is shown in Lee *et al* (2006)

Finally, an outstanding pitfall to be avoided is the over-interpretation of poorly fitted data which must always be treated with great caution. Because particle scattering spectra are not easily inverted into depth profiles since the signal at a particular channel can come from various elements at different depths, if the spectrum is poorly fitted the model may be *entirely wrong!* In particular, the fact that a *part* of the spectrum can be perfectly fitted does *not* mean that the model is partly correct! A particle scattering spectrum is an object with some holographic properties: its parts are interdependent. Of course, no spectrum is perfectly fitted, but the analyst should ensure both that the fit is qualitatively correct *for the entire spectrum* and that misfitting regions are understood properly. For example, the low energy signal is not usually well fitted since multiple, plural and slit scattering effects are generally neglected.

There are two main conclusions: **Reliable analysis requires well fitted data.** However, a well-fitted spectrum implies *only* the **validity** of the model, and *not* its **truth**.

6 Unwanted Target-Beam Interactions

6.1 Beam-Induced Heating

The power deposited in a target under beam impact is expressible in watts through the product of the particle energy (MeV) and the number of particles per second (μA), where the latter represents particle current, not electrical current. If the cross sectional area of the beam is known, then the power density (watts per unit area) is also readily calculated. Basic heat flow calculations can then be made.

For a target of semi-infinite thickness, the validity of this calculation rests on the fact that the fraction of incident particles reflected or scattered out of the target is negligible (< 1%), which is satisfied for all beams at MeV energies. It further requires that secondary particle emission (sputtered particle flux, nuclear reaction product flux, electron emission, etc.) produces no secondary heating effects. Again, for MeV particles, this assumption is usually satisfied. For thin targets, the heat input is determined by the energy deposited by the beam within the target; this may be much less than the incident energy. While it is usually of no interest in ion beam analysis applications, heat generation in the target will proceed via the same fundamental interactions that have been identified in discussions of 'spike' phenomena. Beam energy expended through electronic stopping is coupled to electrons, that is, the electrons are 'heated' and this excitation must then be coupled to the lattice through electron-phonon interactions, thereby producing macroscopic sample heating with a characteristic time constant of picoseconds. The route to lattice heating is more direct in the nuclear stopping regime, which dominates near the end of the particle range. As noted above, however, the quantity of interest is usually the mean power deposited. The variation in rate of thermalization of the lattice with depth is rarely of concern.

The sample response to beam heating depends on experimental conditions. If the beam spot is small in area, radial symmetry may be assumed. At temperatures above a few hundred degrees centigrade, cooling will be dominated by the radiative mechanism (T^4) rather than by conduction. (When conductivity within the sample is good, temperature profiles will be rather unremarkable.)

However, mechanical contact does not ensure good **thermal** contact, and thermal contacts are notoriously hard to make in a vacuum. The existence of a hot spot can lead to differences in

- Electron emission;
- Sticking probabilities for adsorbates (e.g. O_2. CO, H_2O, etc.) and thus lower coverages relative to cooler surrounding material;
- Varying decomposition rates for adsorbed hydrocarbons; and
- Annealing of beam-induced disorder.

Thermal gradients can result in redistribution of mobile impurities, including embedded gas atoms from the beam, and can decompose materials. The question of how best to determine the target temperature under the beam lies outside the scope of these comments. Schultz *et al,* (1992) has shown how important temperature control can be: large changes (up to an order of magnitude) in the level of residual disorder in MeV energy self-irradiation of Si over the temperature range 270K-320K for otherwise identical irradiation conditions have been observed. Hence, significant changes in beam-induced disorder may result from beam heating of even a few degrees.

It is worth emphasising that beam induced heating effects are exacerbated when a microbeam is used.

6.2 Beam-Induced Radiation Damage

In many IBA applications, radiation damage produced by the ion beam is a key limitation. In general, such effects depend not only on the primary energy loss process involved, but also on subsequent solid state diffusion effects. Hence, the nature and temperature of the target, the dose rate, and the total fluence are all relevant parameters. The review literature on radiation damage is extensive (see for example Grubb 1974, Weber *et al*. 1997, Averback & de la Rubia 1998) and we give here only some simple guidelines to assist newcomers in the IBA field.

Radiation damage processes arise from two widely different mechanisms of energy transfer:

- Nuclear (or atomic) stopping, $(dE/dx)_n$, in which scattering of the incident ion by the (partially-) screened target nucleus results in significant momentum being transferred to the whole atom. This contribution is the dominant energy-loss process at low (keV) energies,

but at energies common in IBA (~1MeV/nucleon) it is only a very small fraction (~0.1%) of the total stopping process.

- Electronic stopping, $(dE/dx)_e$, in which energy is lost to various electronic excitation and ionization processes.

In metals and most semiconductors, electronic excitation and ionization both decay almost instantaneously without producing permanent damage effects. In such materials, the major source of radiation damage is the small nuclear stopping component (first mechanism, above). An upper limit to the resulting defect density may be obtained by multiplying the nuclear stopping power, $(dE/dx)_n$ ($eV.10^{-15}cm^2$), by the total ion fluence and dividing by twice the displacement energy, E_d. At IBA energies, the nuclear stopping power is usually between 0.03 and 0.3 $eV.10^{-15}cm^2$ and E_d is typically -30 eV. Hence, a beam fluence of 10^{15} ions cm^{-2} produces at most a defect density in the 0.05-0.5% range.

On the other hand, in insulators and other molecular compounds, damage production rates are often considerably greater because here the electronic stopping power (second mechanism, above) may also cause bond breakage and hence permanent chemical and structural changes in the target. Radiation chemistry studies in a wide variety of inorganic and organic molecular solids, using e^-, γ–ray, and MeV ion bombardment, have shown that the number of bonds broken per 100 eV of deposited energy (the so-called g-factor) is roughly 10, indicating that in such materials electronic stopping processes are usually more effective in breaking bonds than the nuclear collision cascades. For example, Benyagoub (2006) shows that the fraction g of electronic energy loss converted to heat is 0.124 for zirconia and 0.129 for hafnia. Since the electronic stopping power at IBA energies is two to three orders of magnitude greater than the nuclear stopping power, it is evident that the total rate of damage creation in insulators can be as much as 10^3 greater than the nuclear collision estimates in the previous paragraph.

In practice, the observed levels of damage vary widely from one type of insulator to another. We have presented here only a rough estimate of the maximum rate at which damage is created; in many materials, self-annealing reduces the damage. For example, most ceramic materials (WC, BN) and certain inorganic oxides (MgO, $A1_2O_3$, SiO_2, UO_2) are fairly resistant, whereas alkali halides, polymers, and most organic and biological materials are rapidly and permanently decomposed by electronic stopping processes. In particular, the beam is actually capable of rapidly drilling holes in PTFE (poly-tetrafluoroethylene) (Grime *et al.*, 2005).

Damage creation due to electronic stopping is not restricted to insulators, but may occur in any polyatomic molecular solid, including high-T_c superconductors.

Finally, it should be emphasized that even when a large amount of damage is created by the analyzing beam, this does not necessarily introduce significant error into the quantities being analyzed. However, if some of the resulting defect species are mobile (radiation-enhanced diffusion) or volatile (for example, H_2), then significant changes in depth distribution or stoichiometry may result. In some cases, low-temperature analysis may reduce the problem.

Single crystal targets, which involve RBS/channelling analyses, are particularly sensitive to all types of radiation damage, even when the resulting defect species are non-mobile. Interaction between solute atoms and point defects (vacancies or interstitials), for example, can cause solute atoms to move into a completely different lattice site configuration (see Chapter 10, Section 10.7.6????).

Again, it is worth emphasising that beam-induced damage effects are exacerbated when a microbeam is used.

6.3 Beam-Induced Sputtering

As part of the radiation damage process, near-surface atoms occasionally receive sufficient kinetic energy or electronic excitation to be ejected — sputtered — from the target surface. Obviously, if the amount sputtered during IBA becomes significant (10^{15} cm^{-2} ~one monolayer), then the surface structure, stoichiometry, film thickness, etc. could be irreversibly changed. Again, as in the radiation damage section (12.5.1.2), we divide the discussion into two widely different types of behaviour.

In metals and most semiconductors, only the nuclear stopping component contributes to sputtering and the observed yield is directly proportional to $(dE/dx)_n$ evaluated at the target surface, that is, at the incident beam energy E_0. The relationship between the sputtering yield, Y (atoms/ incident ion), and $(dE/dx)_n$ ($eV/10^{15}$ atoms cm^{-2}) can be expressed as

$$Y = 0.1(dE/dx)_n / (U_s \cos\phi) \qquad (4)$$

The numerator *[0.1 $(dE/dx)_n$]* is a rough estimate of the total energy (in eV) contributing to the sputtering process, U_s (the surface binding energy of the target) is usually between 2 and 10 eV/atom, and ϕ is the angle between the incident beam direction and the surface normal. Andersen (1987) shows, fortuitously, an exceptionally good theoretical description of the sputtering behaviour of Ni (a typical metal) as a function of the energy and atomic number of the incident beam. The maximum sputtering yield is about 10^{-2}Ni/incident ion for about 1keV H, and about 8Ni/ion for 100keV Xe. In general however, the agreement between predicted and measured sputtering yields is no better than a factor of two.

In the low-E regime (10-100 keV) where $(dE/dx)_n$ reaches its maximum value, sputtering yields as large as 10 atoms/ion are often encountered. But at IBA energies, $(dE/dx)_n$ is in the range of 0.03-0.3 $eV/10^{15}$ atoms/ cm^{-2}; hence, the sputtering yield is less than 10^{-2}.

In insulators, the collision cascade mechanism of sputtering (described above) still occurs and hence sputtering yields of at least 10^{-3} atoms/ion occur in all IBA studies. In insulators, however, the much larger $(dE/dx)_e$ process can also produce significant sputtering through a variety of mechanisms: bond breaking, 'Coulomb explosion' effects, formation of volatile products (H_2, O_2, etc.). The exact mechanisms are, in general, not well characterized and they depend markedly on the type of insulating material involved. Nevertheless, experimental evidence (Tombrello, 1984) shows that the sputtering yield in insulators can be as high as 10 (in rare cases, even 100) atoms/incident ion. In such materials, the electronic stopping process has enhanced the sputtering rate by as much as 10^4.

Note that in polyatomic targets, preferential sputtering of certain atomic species can often occur. Hence, whenever the total amount sputtered is greater than one monolayer (~10^{15} cm^{-2}), significant changes in near-surface stoichiometry may also result. An extreme example is the rapid dehydrogenation (or graphitization) of polymers that occurs during IBA with MeV He^+ beams (see, for example, the review of polymer damage by Brown in 1986).

6.4 Charging in Insulators

Compared to metals and semiconductors, most insulating materials present a series of special problems in regard to IBA. In the preceding section (12.5.1) on beam-induced damage, the greatly enhanced sensitivity of insulators to beam-induced effects such as radiation damage and sputtering has already been emphasized. Here, we briefly note two additional complications that arise in certain types of insulating materials: target charging and photon emission.

Depending on the geometry, thickness and resistivity of the target material, surface charging under MeV ion bombardment can in severe cases reach several tens of kV. (This value is, of course, still small compared to the incident beam energy, unlike the insulator situation encountered in Auger and secondary ion mass spectroscopy.) However, since the charge states of the incident and

backscattered beam are not necessarily the same, surface charging can seriously distort the energy and hence the shape of the observed RBS spectrum, as shown for the case of quartz in Fig.7.

Furthermore, surface charging sometimes produces sufficiently high electric fields to interfere with the performance of the Faraday cup system. Also, in certain insulators (for example, $BaTiO_3$), excessive surface charging may even cause the target to disintegrate.

One effective way to neutralize surface charging effects is to provide a supply of low-E electrons from a small, hot filament located nearby. If such a filament is powered via an isolation transformer and is electrically connected to the target holder through a suitable (+50V) bias to prevent electrons escaping to the chamber walls, then quantitative current integration is still achievable.

Generally, the use of a transmission Faraday cup is a better way to solve these current integration problems.

Other possible methods that have been used to reduce surface charging are:

- Coating the surface at least partially with a very thin layer of conducting material, such as graphite (for example, rubbing a pencil lightly across the surface sometimes works) or an evaporated metal (or carbon).
- Sweeping the beam so that it also bombards the adjacent (metal) target holder or a suitably placed metal grid in front of the target. The latter process generates a supply of secondary electrons to neutralize the positively charged surface of the insulator.

In many insulators, charging effects are small enough to be ignored, or discharge by surface tracking can be encouraged by analysing close to a contact.

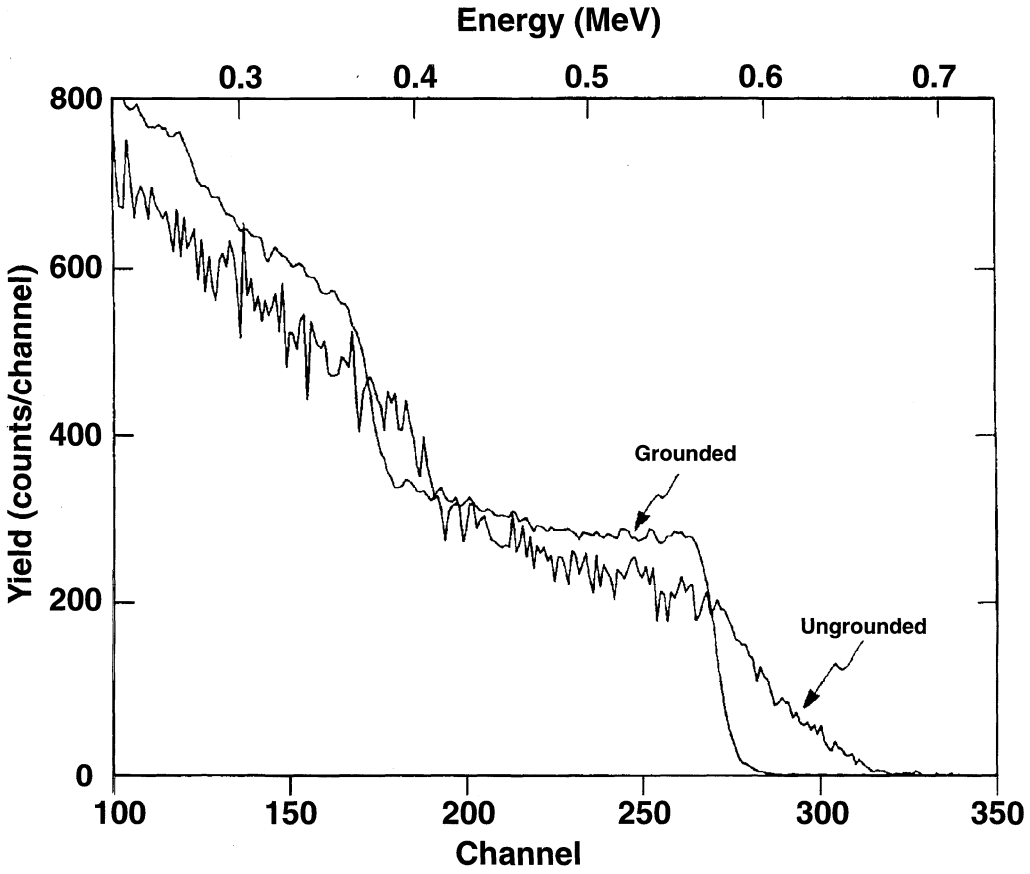

Figure 7. Surface charging effect. Comparison of RBS spectra from a quartz target using 1 MeV ^{4}He: a) ungrounded; b) grounded via a thin conductive surface layer of graphite by rubbing a pencil lightly across the surface (Almeida and Macauley-Newcombe, private communication, 1991).

6.5 Photon Emission in Insulators

In insulators, much of the electronic excitation resulting from the $(dE/dx)_e$ stopping mechanism is eventually converted into optical emission in the visible and ultra violet region. Polymers, alkali halides, etc. are transparent to such radiation. Consequently, photons emitted even from a depth of several microns can readily escape from the target. In such cases, hundreds or even thousands of photons may be emitted per incident ion. We have already discussed how these photons can generate a flux of secondary electrons at the chamber walls. Furthermore, the energy resolution of charged-particle detectors can be seriously degraded by photogeneration of carriers in the depleted region. (The standard surface barrier detector has a Au electrode of thickness ~20nm which is transparent to visible light.)

7 Other Effects

7.1 Surface and Interface Roughness

When performing experiments where the incident or emergent charged particle makes a small angle (for example < 15°) with a target surface which is not smooth, problems in the shape of the energy distribution may arise that are caused by the surface topography. This is very often the case for ERDA measurements (see Chapter 5). Even at near-perpendicular incidence, porous targets, sintered powders, etc. can introduce very serious surface roughness complications, leading to data that either are impossible or troublesome to analyse or that do not carry useful information. Recently Molodtsov *et al* (2008) have shown how to handle spectra from very rough samples, but this algorithm is not yet implemented in IBA codes.

When roughness is moderate (that is, when it is not so much that it destroys spectral features), IBA can be used effectively to study surface and interfacial roughness. Different methods have been developed. The simplest one is to average spectra calculated for different sample structures, e.g. if the roughness leads to a layer with changing thickness. Full Monte Carlo simulations have also been made. A fast and often efficient approach is to calculate the broadening of observed features due to specific types of roughness. Calculations of the effect of voids, inclusions, and quantum dots, are also included in some codes (see Barradas, 2001, and Mayer *et al*, 2005).

However, it is normally impossible to determine from IBA techniques alone whether the broadening of a given peak or edge is due to roughness, to interdiffusion, or to an unexpected depth profile of the affected element. Interpretation of the data almost always requires extra information about the sample at hand from some other source. Different microscopies are often employed for that purpose.

7.2 Target Non-Uniformity

Care must be taken in resting the interpretation of RBS spectra on limited data. Apparently simple features may be misleading if it is assumed that the target has lateral uniformity under the analyzing beam. As shown by Campisano *et al.* (1975), the shape of a Pb spectrum recorded from a non-uniform surface film of Pb on Si may closely resemble that of a laterally uniform diffusion profile of Pb in Si.

This confusion is removed by supplementary measurements and analysis (Campisano *et al.,* 1978). As shown in Fig.8a, the consequences of varying the target angle, ϕ, to the incident beam for a Pb film of thickness 50 nm overlaying an Si substrate are to give a familiar $(\cos\phi)^{-1}$ broadening of the Pb profile in the RBS spectrum, and a correlated shift in the leading edge of the Si continuum. Totally different profiles are obtained for samples which have been annealed to 280°C for 20 minutes, after deposition. In this case (Fig.8b), the decrease in the scattered particle yield, $H_{Si,}$ from Si atoms at the surface as the tilting angle (ϕ) increases rules out interdiffusion. The results have been

modelled in terms of raised Pb features (islands) and good agreement found with island dimensions and spacings measured by SEM analysis which displays the altered surface morphology. RBS methods have been used very effectively (Zinke-Allmang *et al,* 1989) to study the development of layer-by-layer and island growth (Stranski-Krastanov films).

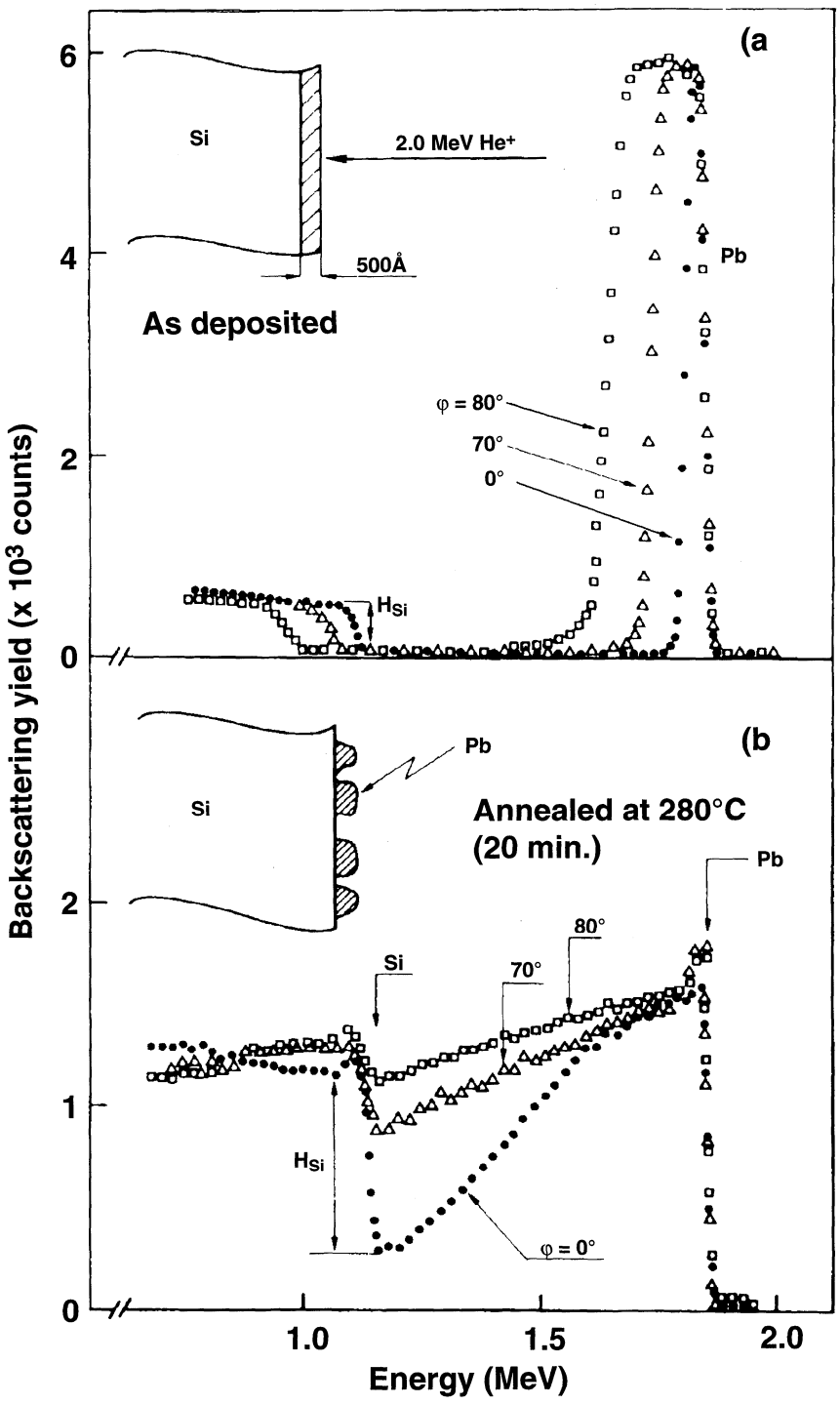

Figure 8: Ambiguity in RBS between roughness and diffusion. Backscattered energy spectra for several tilting angles, a) From a uniform Pb layer (50nm) on a Si substrate; and b) from the same layer after annealing for 20 minutes at 280°C (Campisano *et al,* 1978).

7.3 Thin Film Units

Thin film units (10^{15}atoms/cm^2) are the natural units for IBA since the energy loss is measured in eV/(atoms/cm^2), and one monolayer is of the order of 10^{15}atoms/cm^2.

The energy loss is measured in these units because the accurate measure of thin film thickness is in terms of μg/cm^2 (equivalent to atoms/cm^2 if the stoichiometry is known) since the most reliable way to measure the thickness of a thin film is to weigh it, and measure its area. Linear thicknesses (in nm) are unreliable because the density of thin films can be markedly different from bulk values, and because surface contamination (including oxides) and other surface effects can be large for thin films.

IBA is an ideal technique to measure thin film profiles where the composition changes with depth. In these cases, the appropriate density to use depends on the chemistry of the sample, and assuming different chemistries will lead one to infer a different density profile. Therefore, the most neutral representation of IBA measured depths is in terms of μg/cm^2; thin film units are very convenient and do not involve the sample density, but do assume that the stoichiometry is known.

The pitfall that must be avoided is to forget that presenting depth profiles with a linear depth scale (in nm) hides assumptions about the density of the sample, which may not be well known, and may be greatly different from what is expected. Some IBA codes allow the analyst to fit the data using molecules, and using mixtures of molecular densities. In Fig.6 for example, the depth scale is in thin film units. To plot the profiles in nm one must correctly assign the oxide densities, which is not entirely trivial.

References

Abel F, Amsel G, d'Artemare E, Ortega C, Siejka J, Vizkelethy G (1990), *Use of the $^{16}O(3He,a)^{15}O$ reaction for studying oxygen-containing thin-films*, Nucl. Instr. and Meth. **B45,** 100-104

Alexander TK, Ball GC, Lennard WN, Geissel H, Mak H-B (1984), *Measurement of the absolute cross-section of the $^3He(^4He,\gamma)^7Be$ reaction at E_{cm} =525 keV*, Nucl Phys. **A427,** 526-544

Alkemade PFA, Habraken FHPM, van der Weg WF (1990), *On the ambiguity in the analysis of Rutherford backscattering spectra*, Nucl. Instr. and Methods **B45** 139-142

Allison SK (1958), *Experimental results on charge-changing collisions of H and He atoms and ions at energies >0.2keV*, Rev.Mod.Phys. 30(4) 1137-1168

Amsel G, Samuel D (1967), *Microanalysis of stable isotopes of oxygen by means of nuclear reactions ,* Anal. Chem. **39**, 1689

Amsel G, Girard E, Vizkelethy G, Battistig G, Girard Y, Szilágyi E (1992), *High pulse-rate and pileup handling in precision RBS,* Nucl. Instrum. Methods **B64**, 811-816

Amsel G, Davies A (1983), *Precision standard reference targets for microanalysis by nuclear-reactions*, Nucl. Instr. and Meth. **218,** 177-182

Andersen HH, Besenbacher F, Loftager P, Möller W (1980), *Large angle scattering of light ions in the weakly screened Rutherford region*, Phys. Rev. A **21** 1891-1901

Andersen HH (1987), *Computer-simulations of atomic-collisions in solids with special emphasis on sputtering,* Nucl. Instr. and Meth. **B18**, 321-343

Arstila K, Sajavaara T, Keinonen J (2001), *Monte Carlo simulation of multiple and plural scattering in elastic recoil detection*, Nucl. Instr. and Meth. **B174** 163-172

Audi G, Wapstrab AH, Thibaulta C (2003), *The AME2003 atomic mass evaluation: (II). Tables, graphs and references*, Nuclear Physics **A729** 337-676

Averback RS, de la Rubia TD (1998), *Displacement damage in irradiated metals and semiconductors*, Solid State Phys. **51**: 281-402

BAM (2009): BAM-S107, BAM-S108, BAM-S109, BAM-S110 in the *Catalogue of Certified Reference Materials* from the Bundesanstalt für Materialforschung und –prüfung (BAM), Berlin

Banks JC, Browning JF, Wampler WR, Doyle BL, LaDuca CA, Tesmer JR, Wetteland CJ, Wang YQ, (2004) *Round robin analyses of hydrogen isotope thin films standards*, Nucl. Instr. and Meth, **B219-220**, 444-449

Barradas NP, Jeynes C, Jenkin M, Marriott PK (1999a), *Bayesian Error Analysis of Rutherford Backscattering Spectra*, Thin Solid Films **343-344** 31-34

Barradas NP, Keddie JL, Sackin R (1999b) *Bayesian inference analysis of ellipsometry data*, Phys.Rev. **E59**(5) 6138-6151 Part B

Barradas NP (2001), *Rutherford backscattering analysis of thin films and superlattices with roughness*, J. Phys. D: Appl. Phys. **34** 2109-2116

Barradas NP (2002), *Fitting of RBS data including roughness: Application to Co/Re multilayers*, Nucl. Instrum. Methods **B190**, 247-251

Barradas NP, C. Jeynes, R.P. Webb, E. Wendler (2002), *Accurate determination of the stopping power of ^{4}He in Si using Bayesian inference*, Nucl. Instr. and Methods **B194** 15-25

Barradas NP (2004), *Double scattering in grazing angle Rutherford backscattering spectra*, Nucl. Instr. and Meth. **B225** 318-330

Barradas NP, M.A.Reis (2006), *Accurate calculation of pileup effects in PIXE spectra from first principles*, X-ray Spectrometry **35(4)**, 232-237

Barradas NP, Arstila K, Battistig G, Bianconi M, Dytlewski N, Jeynes C, Kótai E, Lulli G, Mayer M, Rauhala E, Szilágyi E, Thompson M (2007), *International Atomic Energy Agency intercomparison of Ion Beam Analysis software*, Nucl. Instrum. Methods **B262:** 281-303; see also Nucl. Instrum. Methods **B266** (2008) 1338-1342

Barradas NP, Jeynes C (2008), *Advanced physics and algorithms in the IBA DataFurnace*, Nucl. Instrum. Methods **B266** 1875-1879

Bauer P, Bortels G (1990), *Response of Si detectors to electrons, deuterons and alpha-particles*, Nucl. Instr. and Meth. **A299,** 205-209

Bauer P, Steinbauer E, Biersack JP (1992), *The width of an RBS spectrum: influence of plural and multiple scattering*, Nucl. Instr. and Methods **B64** 711-715

Bauer P, Steinbauer E, Biersack JP (1993), *RBS beyond the single scattering model*, Nucl. Instr. and Methods **B79** 443-445

Benyagoub A (2006), *Phase transformations in oxidesinduced by swift heavy ions*, Nucl.Instrum.Methods **B245**, 225-230.

Bianconi M, Abel A, Banks JC, Climent Font A, Cohen C, Doyle BL, Lotti R, Lulli G, Nipoti R, Vickridge I, Walsh D, Wendler E (2000), *The Si surface yield as a calibration standard for RBS*, Nucl. Instr. and Methods **B161-163** 293-296

Blaauw M, Campbell JL, Fazinić S, Jakšić M, Orlic I, Van Espen P (2002), *The 2000 IAEA intercomparison of PIXE spectrum analysis software*, Nucl. Instr. and Meth., **B189**, 113-122

Brice DK, Doyle BL (1990), *A curved detection slit to improve ERD energy and depth resolution*, Nucl.Instrum.Methods **B45**, 265-269

Brown WL (1986), *Ion-bombardment effects in polymers*, Rad. Eff. **98,** 115-137

Butler JW (1990), *Criteria for validity of Rutherford scatter analysis*, Nucl. Instrum. Methods **B45** 160–5

Boudreault G, Claudio G, Jeynes C, Low R, Sealy BJ (2004a), *Accurate calibration of the retained fluence from a versatile single wafer implanter using RBS*, Nucl.Instrum.Methods **217** (1): 177-182

Boudreault G, Elliman RG, Grötzschel R, Gujrathi SC, Jeynes C, Lennard WN, Rauhala E, Sajavaara T, Timmers H, Wang YQ, Weijers TDM (2004b), *Round robin: measurement of H implantation distributions in Si by elastic recoil detection*, Nucl. Instr. and Meth. **B222**, 547-566

Campisano SU, Foti G, Grasso F, Rimini E (1975), *Determination of concentration profile in thin metallic-films - applications and limitations of He+ backscattering*, Thin Solid Films **25,** 431-440

Campisano SU, Ciavola G, Costanzo E, Foti G, Rimini E (1978), *Tilting angle dependence of Rutherford backscattering - uniformity of near-surface layers*, Nucl. Instr. and Meth. **149,** 229-233

Christensen NS, Jensen F, Besenbacher F, Stensgaard I (1990), *Absolute calibration of the $^{18}O(p, a_0)^{15}N$ nuclear-reaction*, Nucl. Instr. and Meth. **B51,** 97-101

Cohen C, Davies JA, Drigo AV, Jackman TE (1983), *Intercomparison of absolute standards for RBS studies*, Nucl. Instr. and Meth. **218,** 147-148

Comedi D, Davies JA (1992), *Pulse-height response of Si surface-barrier detectors to 5-70-MeV heavy-ions*, Nucl. Instr. and Meth. **B67,** 93-97

Davies JA, Norton PR (1980), *Absolute coverage measurement of adsorbed Co and D_2 on platinum*, Nucl. Instr. and Meth. **168,** 611-615

Davies JA, Jackman TE, Eschbach HL, Domba W, Wätjen U, Chivers D (1986), *Calibration of the Harwell series II Si-implanted RBS standards*, Nucl. Instr. and Meth. **B15,** 238-240

Doolittle LR, *Algorithms for the rapid simulation of Rutherford backscattering spectra* (1985), Nucl. Instr. and Meth. B9 344-351; Doolittle LR, *A semiautomatic algorithm for Rutherford backscattering analysis*, Nucl. Instr. and Meth. **B15** (1986) 227-231

Edge RD (1983), *RBS microscopic "Tomography"*, IEEE Trans.Nucl.Sci. **NS-30** (2) 1685-1687

El Bouanani M, Pelicon P, Razpet A, Čadež I, Budnar M, Simčič J, Markelj S (2006), *Simple and accurate spectra normalization in ion beam analysis using a transmission mesh-based charge integration* Nucl.Instrum.Methods **B243** 392-396

Eckstein W, Mayer M (1999), *Rutherford backscattering from layered structures beyond the single scattering model*, Nucl. Instr. and Methods **B153** 337-344

Ecker KH, Wätjen U, BergerA, Persson L, Pritzkow W, Radtke M, Riesemeier H (2002), *RBS, SY-XRF, INAA and ICP-IDMS of antimony implanted in silicon – a multi-method approach to characterize and certify a reference material*, Nucl. Instr. and Methods **B188** 120-125

Fischer R, Mayer M, von der Linden W, Dose V (1997), *Enhancement of the energy resolution in ion-beam experiments with the maximum-entropy method*, Phys.Rev.E **55** 6667- 6673

Geissel H, Lennard WN, Ball GC, Forster JS, Lone MA, Milani L, Phillips D, Plattner HH (1984), *Influence of 1.3 MeV ^{4}He post-bombardment on the depth profiles of 35 keV ^{3}He ions implanted into Nb and Au***,** Nucl. Instr. and Meth. **230,** 770-773

Pascual-Izarra C, Barradas NP (2008), *Introducing routine pulse height defect corrections in IBA*, Nucl. Instrum. Methods Phys. Res. **B266** 1866-1870

Giuntini L, Mando PA (1994), *External beam RBS in an unenclosed He environment*, Nucl. Instrum. Methods **B85**, 744-748

Goulding FS, Landis DA (1982), *Signal Processing for Semiconductor Detectors*, IEEE Trans. Nuc. Sci., **NS-29**, 1125-1141

Grime GW, Sofield CJ, Gomez-Morilla I, Gwilliam R, Ynsa MD, Enguita O (2005), *Rapid direct micromachining of PTFE using MeV ions in an oxygen rich atmosphere*, Nucl. Instr. Meth. **B231**, 378-383. This effect has also been observed in a poor vacuum.

Grubb DT (1974), *Review: Radiation-damage and electron-microscopy of organic polymers*, J.Mat.Sci. **9** (10): 1715-1736;

"GUM:1995" BIPM/IEC/IFCC/ISO/IUPAC/IUPAP/OIML "*Guide to the expression of uncertainty in measurement*". Identical to EN 13005:1999. See also the valuable websites www.gum.dk, www.npl.co.uk/scientific_software/research/uncertainties.

Gurbich AF, Kornilov NV (1991), *Backscattering spectrometry with time-of-flight pileup rejection*, Nucl.Instrum.Methods **B62**, 151-154

Gurbich AF (1995), *On the origin of the low energy tail in charged particle spectra*, Nucl. Instr. and Methods **A364** 496-500

Gurbich AF (1996), *Pile-up suppression in backscattering spectrometry using particle identification technique*, Nucl.Instrum Methods **B111**, 137-140

Gurbich AF (1997), *Evaluation of non-Rutherford proton elastic scattering cross section for oxygen*, Nucl.Instrum Methods **B129** 311-316

Gurbich AF (1998), *Evaluation of non-Rutherford proton elastic scattering cross section for carbon*, Nucl.Instrum Methods **B136–138** 60-65

Gurbich AF (2000), *Evaluation of the cross-section for elastic scattering of ^{4}He from carbon,* Nucl.Instrum Methods **B161-163** 125-129

Gurbich AF, Molodtsov SL (2004), *Application of IBA techniques to silicon profiling in protective oxide films on a steel surface,* Nucl. Instr. and Meth. **B226** 637-643

Gurbich AF (2004), *On the concept of an actual Coulomb barrier*, Nucl. Instr. and Meth. **B217**: 183-186

Gurbich A, Jeynes C (2007), *Evaluation of non-Rutherford proton elastic scattering cross section for magnesium*, Nucl. Instr. and Meth **B265**, 447-452

Gurbich A (2008), *Evaluation of non-Rutherford proton elastic scattering cross section for nitrogen*, Nucl.Instrum Methods **B266** 1193-1197

Hemment PLF, Singleton JF, Stephens KG (1975), *Effect of poor vacuum conditions on analysis of thin films by RBS,* Thin Solid Films **28**, L1-L4

Hautala M, Luomajarvi M (1980), *Correction of the Rutherford scattering cross-section in the backscattering analysis*, Rad. Eff. **45,** 159-162

Huenges E, Rösler H, Vonach H (1973), *High-resolution time-of-flight system for precise measurement of excitation energies and Q-values*, Physics Letters **B46(3)** 361-363

IBANDL (2009) database at www-nds.iaea.org/ibandl maintained by A.F.Gurbich.

ICRU Report 49 (1993), International Commission on Radiation Units and Measurements, Bethesda, MD, USA.

Jeynes C, Kimber AC (1985), *High accuracy data from Rutherford backscattering spectra: Measurements of the range and straggling of 60-400 keV As implants into Si*, J. Phys. D. **18** L93-L97

Jeynes C, Jafri ZH, Webb RP, Ashwin MJ, Kimber AC (1997), *Accurate RBS measurements of the In content of InGaAs thin films,* Surf. Interface Anal. **25** 254–60

Jeynes C, Barradas NP, Blewett MJ, Webb RP (1998), *Improved ion beam analysis facilities at the University of Surrey*, Nucl. Instr. and Methods **B136-138** 1229-1234

Jeynes C, Barradas NP, Marriott PK, Boudreault G, Jenkin M, Wendler E, Webb RP (2003), *Elemental thin film depth profiles by ion beam analysis using simulated annealing - a new tool*, J.Phys.D: Appl.Phys. **36** R97-R126

Jeynes C, Peng N, Barradas NP, Gwilliam RM (2006), *Quality assurance in an implantation laboratory by high accuracy RBS*, Nucl. Instrum. Methods **B249**: 482-485

Kirkpatrick S, Gelatt Jr. CD, Vecchi MP (1983), *Optimization by Simulated Annealing*, Science **220** 671-680

Konac G, Kalbitzer S, Klatt C, Niemann D, Stoll R (1998), *Energy loss and straggling of H and He ions of keV energies in Si and C*, Nucl. Instr. and Meth. **B136-138** 159-165

Knoll GF (1989), *Radiation Detection and Measurement*, 2nd edition, John Wiley and Sons, New York

L'Ecuyer J, Davies JA, Matsunami N (1979), *How accurate are absolute Rutherford backscattering yields*, Nucl. Instr. and Meth. **160,** 337-346

Lee WP, Gundabala VR, Akpa BS, Johns ML, Jeynes C, Routh AF, (2006), *Distribution of surfactants in latex films: A Rutherford backscattering study*, Langmuir **22** 5314-5320

Lennard WN, Geissel H, Winterbon KB, Phillips D, Alexander TK Forster JS (1986), *Nonlinear response of Si detectors for low-Z ions*, Nucl. Instr. and Meth. **A248,** 454-460

Lennard WN, Tong SY, Mitchell IV, Massoumi GR (1989), *An alternative technique for oxygen-surface coverage measurements*, Nucl. Instrum. Methods. **B43**, 187-193

Lennard WN, Massoumi GR (1990), *Anomalous pulse heights in silicon detectors*, Nucl. Instr. and Meth. B**48**, 47-50

Lennard WN, Massoumi GR, Simpson TW, Mitchell IV (1999), *Improved stoichiometry measurements using ^{4}He backscattering: experiment and simulation*, Nucl. Instrum. and Methods **B152** 370-376

Marion JB (1966), *Accelerator Calibration Energies*, Rev.Mod.Phys. **38** 660-668

Mattauch JHE, Thiele W, Wapstra AH (1965), *Adjustment of relative atomic masses*, Nucl.Phys., **67**, 73-120

Mayer M, Fischer R, Lindig S, von Toussaint U, Stark RW, Dose V (2005), *Bayesian reconstruction of surface roughness and depth profiles*, Nucl. Instr. Meth. **B228** 349

Mendenhall MH, Weller RA (1991), *Algorithms for the rapid computation of classical cross-sections for screened Coulomb collisions*, Nucl. Instr. and Meth. **B58,** 11-17

Möller W, Besenbacher F (1980), *Note on the 3He+d nuclear-reaction cross-section*, Nucl. Instr. and Meth. **168,** 111-114

Molodtsov SL, Gurbich AF, Jeynes C (2008), *Accurate ion beam analysis in the presence of surface roughness*, J. Phys. D: Appl. Phys. **41,** 205303 (7pp)

Morrison R (2007), *Grounding and Shielding : Circuits and Interference*, Wiley

Munnik F, Plompen AJM, Räisänen J, Wätjen U (1996) , *Stopping powers of 200-3000 keV ^{4}He and 550-1750 keV ^{1}H ions in Vyns*, Nucl. Instr. and Methods **B119**, 445-151

Niemann D, Konac G, Kalbitzer S (1996), *Stopping power measurements of ^{1}H, ^{4}He, and ^{14}N in the energy range of 0.02 - 1 MeV/amu*, Nucl. Instr. and Methods **B118** 11-18

Pászti F, Manuaba A, Hajdu C, Melo AA, Da Silva MF (1990), *Current measurement on MeV energy ion beams*, Nucl. Instrum. Methods **B47** 187-192

Paul H, Schinner A (2001), *An empirical approach to the stopping power of solids and gases for ions from Li to Ar*, Nucl. Instr. Methods Phys. Res. **B179** 299-315

Paul H, Schinner A (2002), *An empirical approach to the stopping power of solids and gases for ions from Li to Ar, Part II*, Nucl. Instr. Methods Phys. Res. **B195** 166-174,

Paul H, Schinner A (2003), *Judging the reliability of stopping power tables and programs for heavy ions*, Nucl. Instr. Methods Phys. Res. **B209** 252-258, see also H. Paul, A. Schinner (2005), *Judging the reliability of stopping*

power tables and programs for protons and alpha particles using statistical methods, Nucl. Instr. Methods **B227** 461-470

Paul H, Schinner A (2006), *Statistical analysis of stopping data for protons and alphas in* compounds, Nucl. Instrum. Methods Phys. Res. **B249** 1-5

Piel N, Berheide M, Polaczyk C, Rolfs C, Schulte WH (1994), *Ion dose determination using beam chopper techniques*, Nucl.Instrum.Methods **A349** (1): 18-26

Pritzkow W, Vogl J, Berger A, Ecker K, Grötzschel R, Klingbeil P, Persson L, Riebe G, Wätjen U (2001), *Contribution of ICP-IDMS to the certification of antimony implanted in a silicon wafer - comparison with RBS and INAA results*, Fresenius J.Anal.Chem, **371** 867-873

Polanyi M (1958), *Personal Knowledge*, Chicago University Press. I quote from the 1974 paperback edition, ch.2, p.19. A beautiful book, invaluable for those who want to know how we know what we know.

Radeka V (1988), *Low-Noise Techniques in Detectors*, Ann. Rev. Nucl. Part. Sci., **38**, 217-277

Reinholz U, Bremser W, Brzezinka KW, Strub E, Weise HP, Merchel S (2008), *A thin-layer reference material for hydrogen analysis*, Nucl. Instr. and Meth. **B266,** 2418-2423

Roush ML, West MA, Marion JB (1970), *Precision determinations of nuclear reaction calibration energies by velocity measurements*, Nucl. Phys. **A147** 235-248

Schultz Peter J, Jagadish C, Ridgway MC, Elliman RG, Williams JS (1991), *Crystalline-to-amorphous transition for Si-ion irradiation of Si(100),* Phys. Rev. **B44,** 9118-9121

Seah MP, David D, Davies JA, Jeynes C, Ortega C, Read PM, Sofield CJ, Weber G (1988), *An intercomparison of absolute measurements of the oxygen and tantalum thickness of tantalum pentoxide reference materials, BCR 261, by 6 laboratories*, Nucl. Instr. and Meth.. **B30,** 140-151

SigmaCalc (2009) database at www-nds.iaea.org/sigmacalc built by A.F.Gurbich.

Sitter C, Davies JA, Jackman TE, Norton PR (1982), *Ultra-high vacuum apparatus for combined low-energy electron-diffraction, Auger-spectroscopy, MeV ion-scattering and nuclear microanalyis*, Rev. Sci. Instr. **53**, 797-802.

Sjöland KA, Munnik F, Chaves C, Wätjen U (1999), *Time-resolved pile-up compensation in PIXE analysis with list-mode collected data*, Nucl. Instr. and Meth **B150**, 69-75

Sjöland KA, Munnik F, Wätjen U (2000), *Uncertainty budget for ion beam analysis*, Nucl. Instrum. Methods **B161** 275-280

Smyth DM (1966), *Heat-treatment of anodic oxide films on tantalum .V: Tthermal redistribution of incorporated phosphorus* , J. Electrochem. Soc. **113,** 1271

Szilágyi E, Pászti F, Amsel G (1995), *Theoretical approximations for depth resolution calculations in IBA methods*, Nucl. Instrum. Methods **B100** 103-121.

Tombrello TA (1984), *Track damage and erosion of insulators by ion-induced electronic processes*, Nucl. Instr. and Meth. **B2**, 555-563

van Lieshout R, Wapstra AH, Ricci RA, Girgis RK (1966), *Scintillation spectra analysi*s, in Siegbahn K (ed.). *Alpha-, beta- and gamma-ray spectroscopy* (North-Holland Publ. Co., Amsterdam): 515-517

Venkatesan T, Brown WL, Wilkens BJ (1984), *Secondary-electron, ion and photon emission during ion-beam irradiation of polymer and condensed gas films*, Nucl. Instrum. Methods **Bl**, 605-609

Wätjen U, Bax H (1994), *Bi-implanted silicon reference material revisited: uniformity of the remaining batch*, Nucl. Instr. and Methods **B85** 627-632

Weber WJ, Ewing RC, Angell CA, Arnold GW, Cormack AN, Delaye JM, Griscom DL, Hobbs LW, Navrotsky A, Price DL, Stoneham AM, Weinberg WC (1997), *Radiation effects in glasses used for immobilization of high-level waste and plutonium disposition*, J.Mat.Res.**12** (8): 1946-1978;

Wielopolski L, Gardner RP (1976) , *Prediction of pulse-height spectral distortion caused by peak pile-up effect***,** Nucl. Instrum. Methods **133** 303-309; R.P. Gardner, L. Wielopolski, *A generalized method for correcting pulse-height spectra for the peak pile-up effect due to double sum pulses*, Nucl. Instrum. Methods **140** (1977) 289-296.

Williams JS, Möller W (1978), *Determination of optimum depth-resolution conditions for Rutherford backscattering analysis*, Nucl. Instr. Meth **157** (2): 213-221

White RE, Barker PH, Lovelock DMJ (1985), *Measurement of Nuclear Reaction Q-values with High Accuracy: $^{7}Li(p,n)^{6}Be$,* Metrologia **21**, 193-199

Ziegler JF (2004), *SRIM-2003*, Nucl. Instr. Meth. **B219-220,** 1027-1030, www.srim.org: